

Creation of turbulence in polyatomic gas flow via an intermolecular potentialRafail V. Abramov ^{*}*Department of Mathematics, Statistics and Computer Science, University of Illinois at Chicago,
851 S. Morgan St., Chicago, Illinois 60607, USA*

(Received 19 January 2022; accepted 10 May 2022; published 25 May 2022)

We develop a tractable interaction model for a polyatomic gas, whose kinetic equation combines a Vlasov-type mean field forcing due to an intermolecular potential, and a Boltzmann-type collision integral due to rotational interactions. We construct a velocity moment hierarchy for the kinetic equation, and find that, under the high Reynolds number condition, the pressure equation becomes decoupled from the angular momentum and stress. For the heat flux, we propose a closure by prescribing the specific-heat capacity of the gas flow. Setting the specific-heat capacity to that of a constant-pressure process leads to the system of equations for a balanced flow, where the momentum transport equation contains the mean field forcing, which is an averaged effect of the intermolecular potential. Remarkably, the balanced flow equations do not contain any information about internal thermodynamic properties of the gas, and are thereby applicable to a broad range of different gases. We conduct numerical simulations for an airlike gas at normal conditions in the inertial flow regime, where the pressure is constant throughout the domain. We find that the presence of the intermolecular potential produces a distinctly turbulent flow, whose time-averaged Fourier spectra of the kinetic energy and temperature exhibit Kolmogorov's power decay.

DOI: [10.1103/PhysRevFluids.7.054605](https://doi.org/10.1103/PhysRevFluids.7.054605)**I. INTRODUCTION**

While turbulent motions in a liquid have first been documented by Leonardo da Vinci, it appears that Boussinesq [1] presented the first systematic account of turbulence in the scientific literature. Six years later, Reynolds [2] demonstrated that an initially laminar flow of a liquid consistently develops turbulent motions whenever the high Reynolds number condition is satisfied. Almost 60 years later, Kolmogorov [3,4,5] and Obukhov [6] observed that the time-averaged Fourier spectra of the kinetic energy of an atmospheric wind possess a universal decay structure, corresponding to the inverse five-thirds power of the Fourier wave number. Numerous attempts to explain the physical nature of turbulence have been made throughout the 20th century [7–21], yet none successfully. Until recently, the physics of turbulence formation in an initially laminar flow, as well as the origin of the power scaling of turbulent kinetic energy spectra, remained unknown. As an example, one can refer to relatively recent works [22,23], where turbulentlike motions in a numerically simulated flow had to be created artificially by deliberate perturbations. In reality, turbulence emerges spontaneously by itself (even if all reasonable measures were taken to preserve the laminarity of the flow, e.g., Reynolds' experiment), which was the primary reason why this peculiar phenomenon attracted worldwide scientific interest to begin with.

In our recent works [24,25], we considered a system of many particles, interacting solely via a repelling short-range potential $\phi(r)$. In the limit of infinitely many such particles, we obtained, via the standard Bogoliubov-Born-Green-Kirkwood-Yvon (BBGKY) formalism [26–28], a Vlasov-type

*abramov@uic.edu

equation [29] for the mass-weighted distribution density of a single particle. This equation contained the mean field potential $\bar{\phi}$, which was the result of the average effect of the short-range potential ϕ . Then, we computed the usual hierarchy of the transport equations for the velocity moments, closed it under the infinite Reynolds number assumption, and arrived at a system of equations for a balanced compressible gas flow.

In [24], we numerically simulated these equations in the inertial flow regime through a straight pipe, with the interaction potential of hard spheres with the mass and diameter corresponding to those of argon. For the initial condition of that simulation, we selected a straight laminar Bernoulli jet, which happens to be a steady state in the conventional Euler equations. We observed, however, that in our simulation such a jet quickly developed into a fully turbulent flow. We also examined the Fourier spectrum of the kinetic energy of the simulated flow, and found that its time average decayed with the rate of inverse five-third power of the wave number, which corresponded to the famous Kolmogorov spectrum. In [25], we extended the framework of [24] onto a gas flow under strong gravity acceleration, which, on a large scale, is effectively two dimensional. We simulated the two-dimensional equations in the inertial and cyclostrophic flow regimes, and found that turbulent motions also appear in an initially laminar flow.

In the past, a similar approach, originating from the basic principles of kinetic theory, was undertaken by Tsugé [30], who attempted to explain the creation of turbulence via long-range correlations between molecules. However, Tsugé's result was restricted to incompressible flow, while, from what we found thus far, it appears that density fluctuations are instrumental in the creation of turbulent dynamics. We have considered long-range interaction effects in our past work [31]; however, from what we later found in [24,25], it appears that even a short-range hard sphere potential is capable of creating turbulence via the mean field effect.

The goal of this work is to extend the turbulent framework of [24,25] onto polyatomic gases. The main challenge with a polyatomic gas is the corresponding kinetic model of interactions between its molecules. Unlike monatomic gases (which can, in many practical situations, be approximated via hard spheres), molecules of polyatomic gases possess rotational degrees of freedom, which store the momentum and energy just like the translational degrees of freedom do. When two such molecules interact, the momentum and energy are exchanged, generally, between linear and angular velocities of both molecules in a complex manner. In order to derive transport equations for a polyatomic gas from kinetic theory, these complex interactions must be described, to a necessary extent, in the context of the kinetic model of intermolecular collisions.

The work is organized as follows. In Sec. II we propose a tractable kinetic model of interactions of polyatomic gas molecules, which combines a deterministic potential with random collisions. In Sec. III we introduce a dynamical system of many molecules which interact according to the aforementioned model, and construct its corresponding forward Kolmogorov equation. In Sec. IV we compute the equation for the statistical distribution of a single molecule, which combines a potential forcing with a Boltzmann-type collision integral, and derive the corresponding system of transport equations of the velocity moments. In Sec. V we decouple the pressure equation from the angular momentum and stress via the high Reynolds number condition, and implement a closure for the divergence of the heat flux by prescribing the specific-heat capacity of the process. For the specific-heat capacity corresponding to that of a process at constant pressure (that is, Charles' law of classical thermodynamics), we arrive at the same system of balanced flow equations as in our recent works [24,25] for monatomic gases. In Sec. VI we show the results of numerical simulations of a turbulent air flow through a straight pipe. We demonstrate that, in the presence of an intermolecular potential, the flow becomes turbulent, and the time averages of the Fourier spectra of its kinetic energy and temperature exhibit a power decay. Section VII summarizes the results of our work.

II. KINETIC MODEL OF INTERACTIONS OF POLYATOMIC MOLECULES

As the first step, we need to formulate a tractable mathematical model of a polyatomic gas on the molecular level. Before proceeding further, however, we have to emphasize that the actual

interaction of atoms is a rather complicated process, which involves quantum-mechanical effects such as the Pauli exclusion. Therefore, what follows has to be interpreted strictly in the context of a vastly simplified, i.e., “mechanical,” model of atomic and molecular interaction, whose purpose is to provide an appropriate formalism which connects the kinetic formulation of the problem and its fluid-mechanical approximation, consistent with fundamental properties of interaction such as the conservation of energy.

In addition to the three usual translational degrees of freedom, each molecule of a polyatomic gas also possesses multiple rotational degrees of freedom, which are capable of storing the momentum and energy. When such molecules interact, they exchange the momentum and energy between all degrees of freedom of both molecules. Unlike monatomic gases, the main challenge with a polyatomic gas is to describe its molecular interactions, which can roughly be separated into two issues.

A. Excessive complexity of a detailed molecular interaction

The first issue to consider with a polyatomic gas is that the exact description of the collision mechanics of two objects beyond that of a pair of hard spheres is excessively complicated for a practical treatment in the context of a kinetic equation. For example, even if two hard spheres are replaced with two rigid ellipsoids (which is a simple topological deformation of a sphere), the collision mechanics already become too complicated to use in a Boltzmann-type collision integral. In particular, not only the actual mechanics of transformation of linear and angular velocities are complex, but even the collision detection criterion is highly nontrivial (as an example, refer to Jia *et al.* [32] and references therein).

B. Effect of Heisenberg’s uncertainty principle

Even if one develops a tractable model of mechanical collisions of two molecules beyond that of hard spheres, there is another difficulty which renders the utility of such model somewhat questionable. Due to Heisenberg’s uncertainty principle, gas molecules cannot be regarded as fully classical objects, especially if the rotational motion of a molecule is involved. Let us look at the following crude estimates of uncertainties associated with the translational and rotational motion:

(i) A molecule of nitrogen (which we take as an example because it is the primary component of air) has the mass of 4.65×10^{-26} kg, which means that the product of the uncertainties in the velocities and coordinates is about 10^{-9} m²/s (the Planck constant divided by the mass). The typical mean-free path between collisions at normal conditions is around 7×10^{-8} m, while the average speed of a molecule at normal temperature is around 500 m/s. Their product is $\sim 10^{-5}$, which gives the relative uncertainty, associated with translational motion, of $\sim 10^{-4}$, or 0.01%.

(ii) At the same time, the size of a molecule of nitrogen is 4×10^{-10} m, which means, that, during the rotation, the two atoms move about each other on this scale. Now, since the kinetic energy of motion is distributed uniformly across translational and rotational degrees of freedom, we have to assume that the atoms of nitrogen move about each other within the molecule at roughly same speeds, that is, ~ 500 m/s. Their product is $\sim 10^{-7}$, which gives the relative uncertainty, associated with rotational motion, of $\sim 10^{-2}$ or 1%.

As we can see, the relative uncertainty associated with rotational motion is about two orders of magnitude larger than that of translational motion, solely due to the corresponding difference in spatial scales (mean-free path vs the molecule size). Note that this difficulty is not related to any interactions, only the fact that the rotational motion of a gas molecule is in itself less deterministic than its translational motion.

C. Our model of interactions between polyatomic molecules

From what is outlined above, the obvious conclusion is not only tracking the angles and angular velocities of molecules, as well as quantifying their collisions in a detailed fashion, is complicated

technically, it is also largely meaningless from the standpoint of physics. Even if one develops a kinetic model which tracks the angular motions and interactions of polyatomic molecules exactly and, deterministically, it is not clear what benefit it would provide if applied to realistic gases at normal conditions. Thus, a reasonable way to proceed from here is to resort to a more general, stochastic model of rotational collisions.

Here, we will take a semiempirical approach to the kinetic description of polyatomic molecular interactions. What this means is that we will formulate a general mathematical model of the interaction of two polyatomic gas molecules with basic properties, but, at the same time, will not elaborate on the specific details of the interaction (as that may be quite complicated). This will lead to a correct mathematical form of the kinetic equation, where the rotational collision integral possesses all necessary general properties. We will neglect interactions of three or more molecules at once: for most gases at normal temperature and pressure, such interactions are not statistically significant.

In the context of our model, the interaction of a gas molecule with another gas molecule can be separated into two distinct effects.

(1) The first effect is the deterministic interaction via an intermolecular potential, where the potential depends only on the translational coordinates, and whose gradient accelerates only the linear velocities. The rotational coordinates and angular velocities are unaffected by the potential interaction.

(2) The second effect is the stochastic collisional interaction, which generally depends on all degrees of freedom, and affects both linear and angular velocities. This effect is responsible for the exchange of the momentum and energy between the linear and angular velocities of both involved molecules.

While the first effect is easy to describe by introducing a suitable intermolecular potential $\phi(r)$, the second effect needs a more detailed elaboration. Namely, we have to formulate a collision model, which is general enough to be capable of describing a broad range of interactions between polyatomic gas molecules, and at the same time is simple enough to be treated analytically to the extent needed. In order to accomplish this, we employ the same mathematical mechanism which we used in our work [33].

In what follows, we assume that collisional interactions occur instantaneously, that is, when a collision occurs, linear and angular velocities of both colliding molecules are changed instantaneously to new values. Thus, the description of a collisional interaction must involve two parts: *when* the interaction occurs, and *how* it occurs. Below, we start with the latter, followed by the former.

D. General mechanics of a polyatomic collision

In what follows, we assume that the total number of degrees of freedom of each gas molecule is N , of which 3 are translational, and $N - 3$ are rotational. We denote the translational coordinates via \mathbf{x} , rotational via \mathbf{y} , while their respective linear and angular velocities are given via \mathbf{v} and \mathbf{w} . Let the linear and angular velocities of the two colliding molecules be denoted via $(\mathbf{v}_1, \mathbf{w}_1)$ and $(\mathbf{v}_2, \mathbf{w}_2)$, respectively. We assume that, whenever the collision occurs, the velocities are changed instantaneously via a collision mapping C to $(\mathbf{v}'_1, \mathbf{w}'_1)$ and $(\mathbf{v}'_2, \mathbf{w}'_2)$, respectively, where the increment depends only on the differences of the precollisional values of the coordinates and velocities, that is,

$$(\mathbf{v}'_1, \mathbf{w}'_1, \mathbf{v}'_2, \mathbf{w}'_2) = C(\mathbf{v}_1, \mathbf{w}_1, \mathbf{v}_2, \mathbf{w}_2) = (\mathbf{v}_1 + \mathbf{g}_{12}, \mathbf{w}_1 + \mathbf{h}_{12}, \mathbf{v}_2 + \mathbf{g}_{21}, \mathbf{w}_2 + \mathbf{h}_{21}). \quad (1)$$

Above, the increments \mathbf{g}_{12} and \mathbf{h}_{12} depend only on the differences between the properties of the two molecules, i.e., they are of the form

$$\mathbf{g}_{12} = \mathbf{g}(\mathbf{x}_1 - \mathbf{x}_2, \mathbf{y}_1 - \mathbf{y}_2, \mathbf{v}_1 - \mathbf{v}_2, \mathbf{w}_1 - \mathbf{w}_2), \quad (2a)$$

$$\mathbf{h}_{12} = \mathbf{h}(\mathbf{x}_1 - \mathbf{x}_2, \mathbf{y}_1 - \mathbf{y}_2, \mathbf{v}_1 - \mathbf{v}_2, \mathbf{w}_1 - \mathbf{w}_2), \quad (2b)$$

with \mathbf{g}_{21} and \mathbf{h}_{21} obviously resulting from inverting the signs of all arguments. From the fundamental principles of physics, the collision must preserve both the linear and angular momenta, as well as the total kinetic energy:

$$\mathbf{v}'_1 + \mathbf{v}'_2 = \mathbf{v}_1 + \mathbf{v}_2, \quad \mathbf{w}'_1 + \mathbf{w}'_2 = \mathbf{w}_1 + \mathbf{w}_2, \quad (3a)$$

$$\|\mathbf{v}'_1\|^2 + \|\mathbf{w}'_1\|^2 + \|\mathbf{v}'_2\|^2 + \|\mathbf{w}'_2\|^2 = \|\mathbf{v}_1\|^2 + \|\mathbf{w}_1\|^2 + \|\mathbf{v}_2\|^2 + \|\mathbf{w}_2\|^2. \quad (3b)$$

The momentum conservation automatically implies

$$\mathbf{g}_{21} + \mathbf{g}_{12} = \mathbf{0}, \quad \mathbf{h}_{21} + \mathbf{h}_{12} = \mathbf{0}, \quad (4)$$

which means that \mathbf{g} and \mathbf{h} are skew symmetric, that is,

$$\mathbf{g}(-\mathbf{z}) = -\mathbf{g}(\mathbf{z}), \quad \mathbf{h}(-\mathbf{z}) = -\mathbf{h}(\mathbf{z}), \quad \mathbf{z} = (\mathbf{x}, \mathbf{y}, \mathbf{v}, \mathbf{w}). \quad (5)$$

We also assume that the mapping C from precollision to postcollision velocities, given via (1), is bijective, that is, there is a unique postcollision state to each precollision state, with a unique inverse. Moreover, the same mapping transforms the negatives of the postcollision velocities into the negatives of the precollision velocities, that is, the negative of C is an involution:

$$-C \circ (-C) = \mathcal{I}. \quad (6)$$

This simply means that if the postcollision velocities are immediately reversed, then the collision occurs in a reverse manner and leads to the reversed precollision velocities. The latter identity, in particular, ensures that the Jacobian of C is unity.

Recall that, in the mechanics of a hard-sphere collision, the collision mapping C itself is also an involution [33,34]. Here, however, we do not make such an assumption since a collision between two polyatomic molecules could be vastly more complicated than a collision between two hard spheres, and it is unclear whether such property would hold.

E. Criterion for triggering a collision

The general mechanics of collision, described above, are deterministic. However, the conditions, under which those collisions occur will be modeled stochastically, as in our recent work [33]. We assume that, when two molecules are sufficiently close to each other (that is, $\|\mathbf{x}_1 - \mathbf{x}_2\|$ is sufficiently small), random collisional interactions may happen with a prescribed conditional intensity. Such artificial randomness reflects the presence of the Heisenberg uncertainty associated with the angular orientation and velocities of the pair of interacting molecules.

Mathematically, the collisions will be triggered via increments of a Poisson process with conditional intensity λ [35,36], where the latter depends on the differences of coordinates and velocities:

$$\lambda_{12} = \lambda(\mathbf{x}_1 - \mathbf{x}_2, \mathbf{y}_1 - \mathbf{y}_2, \mathbf{v}_1 - \mathbf{v}_2, \mathbf{w}_1 - \mathbf{w}_2). \quad (7)$$

This conditional intensity must satisfy the following properties:

- (1) λ is invariant with respect to the reordering of the molecules, that is,

$$\lambda(-\mathbf{x}, -\mathbf{y}, -\mathbf{v}, -\mathbf{w}) = \lambda(\mathbf{x}, \mathbf{y}, \mathbf{v}, \mathbf{w}). \quad (8)$$

- (2) λ is the same for reversed postcollision velocities, that is,

$$\lambda(\mathbf{x}, \mathbf{y}, -\mathbf{v}', -\mathbf{w}') = \lambda(\mathbf{x}, \mathbf{y}, \mathbf{v}, \mathbf{w}) \quad (9)$$

since, for the same angles, in the time-backward configuration the collision must be as likely to occur as in the time-forward configuration.

In what follows, we will generally presume that λ is zero when the two molecules are spaced apart by a considerable distance, so that the collisions are not triggered. Once the molecules approach each other, λ becomes nonzero, thus possibly triggering collisions. The dependence of λ on the angular coordinates and velocities additionally provides for configuring the fine details of a collision

criterion, however necessary. For additional convenience, here we impose the following simplifying assumption on λ :

$$\lambda(\mathbf{x}, \mathbf{y}, \mathbf{v}', \mathbf{w}') = \lambda(\mathbf{x}, \mathbf{y}, \mathbf{v}, \mathbf{w}), \quad (10)$$

that is, the intensity of collisions does not change due to a collision, which, particularly, may result in more than one rotational collision interaction during a single pass of one molecule by another. The latter assumption leads, together with (8) and (9), to λ being fully symmetric under the collisions and reordering of molecules:

$$\begin{aligned} \lambda(\mathbf{x}, \mathbf{y}, \mathbf{v}, \mathbf{w}) &= \lambda(\mathbf{x}, \mathbf{y}, \mathbf{v}', \mathbf{w}') = \lambda(\mathbf{x}, \mathbf{y}, -\mathbf{v}, -\mathbf{w}) = \lambda(\mathbf{x}, \mathbf{y}, -\mathbf{v}', -\mathbf{w}') = \lambda(-\mathbf{x}, -\mathbf{y}, \mathbf{v}', \mathbf{w}') \\ &= \lambda(-\mathbf{x}, -\mathbf{y}, \mathbf{v}, \mathbf{w}) = \lambda(-\mathbf{x}, -\mathbf{y}, -\mathbf{v}', -\mathbf{w}') = \lambda(-\mathbf{x}, -\mathbf{y}, -\mathbf{v}, -\mathbf{w}). \end{aligned} \quad (11)$$

This symmetry is markedly different from the setting we previously used for the random hard-sphere collisions in [33], where the conditional intensity of the Poisson process was set to zero in a postcollision state. In the present context, however, the molecules are repelled via the intermolecular potential ϕ (which was absent in [33]), while the collisions are only used to model additional interactions emerging from the presence of rotational degrees of freedom. Thus, we do not find the condition in (10) too restrictive.

III. DYNAMICAL SYSTEM OF POLYATOMIC MOLECULES

With what is formulated above, the evolution equations for a system of K polyatomic molecules, whose linear and angular coordinates and velocities are expressed via $\mathbf{x}_i, \mathbf{y}_i, \mathbf{v}_i$, and \mathbf{w}_i , are given via the following Lévy-type Feller process [37–40]:

$$\frac{d\mathbf{x}_i}{dt} = \mathbf{v}_i, \quad \frac{d\mathbf{y}_i}{dt} = \mathbf{w}_i, \quad (12a)$$

$$d\mathbf{v}_i = \sum_{j \neq i} \left[-\frac{\partial}{\partial \mathbf{x}_i} \phi(\|\mathbf{x}_i - \mathbf{x}_j\|) dt + \int_{\mathbb{R}^{>0}} \mathbf{g}_{ij} \xi M_{ij}(dt, d\xi) \right], \quad (12b)$$

$$d\mathbf{w}_i = \sum_{j \neq i} \int_{\mathbb{R}^{>0}} \mathbf{h}_{ij} \xi M_{ij}(dt, d\xi). \quad (12c)$$

Above, $\phi(r)$ is the intermolecular potential, and $M_{ij}(t, \cdot)$ is a Poisson random measure with the intensity λ_{ij} , which models rotational collisions between the i th and j th molecules. In a similar manner as in [24,31,33], we concatenate

$$\mathbf{X} = (\mathbf{x}_1, \mathbf{y}_1, \dots, \mathbf{x}_K, \mathbf{y}_K), \quad \mathbf{V} = (\mathbf{v}_1, \mathbf{w}_1, \dots, \mathbf{v}_K, \mathbf{w}_K), \quad (13)$$

and denote

$$\Phi(\mathbf{X}) = \sum_{i=1}^{K-1} \sum_{j=i+1}^K \phi(\|\mathbf{x}_i - \mathbf{x}_j\|), \quad \mathbf{G}_{ij} = (\mathbf{0}, \dots, \mathbf{0}, \mathbf{g}_{ij}, \mathbf{h}_{ij}, \mathbf{0}, \dots, \mathbf{0}, \mathbf{g}_{ji}, \mathbf{h}_{ji}, \mathbf{0}, \dots, \mathbf{0}), \quad (14)$$

where \mathbf{g}_{ij} and \mathbf{h}_{ij} occupy the slots corresponding to \mathbf{v}_i and \mathbf{w}_i , respectively, while \mathbf{g}_{ji} and \mathbf{h}_{ji} occupy the slots corresponding to \mathbf{v}_j and \mathbf{w}_j , respectively, with $i < j$. Then, the dynamical system in (12) can be written in the form

$$d \begin{pmatrix} \mathbf{X} \\ \mathbf{V} \end{pmatrix} = \begin{pmatrix} \mathbf{V} \\ -\partial \Phi / \partial \mathbf{X} \end{pmatrix} dt + \sum_{i=1}^{K-1} \sum_{j=i+1}^K \int_{\mathbb{R}^{>0}} \begin{pmatrix} \mathbf{0} \\ \mathbf{G}_{ij} \end{pmatrix} \xi M_{ij}(dt, d\xi). \quad (15)$$

Obviously, the system above preserves the total energy of the system along its trajectory,

$$E = \frac{1}{2} \|\mathbf{V}(t)\|^2 + \Phi(\mathbf{X}(t)) = \text{const}, \quad (16)$$

which follows from the fact that the collisions preserve the kinetic energy part of the above expression, and do not affect the coordinates.

A. Forward Kolmogorov equation and its steady states

The time derivative of the conditional expectation of a test function ψ is given via the infinitesimal generator of (15),

$$\frac{\partial}{\partial t} \mathbb{E}[\psi] = \mathbf{V} \cdot \frac{\partial \psi}{\partial \mathbf{X}} - \frac{\partial \Phi}{\partial \mathbf{X}} \cdot \frac{\partial \psi}{\partial \mathbf{V}} + \sum_{i=1}^{K-1} \sum_{j=i+1}^K \lambda_{ij} [\psi(C_{ij}(\mathbf{V})) - \psi(\mathbf{V})], \quad (17)$$

where C_{ij} is the collision mapping for the i th and j th velocities. For details on the infinitesimal generators of Lévy-type Feller processes, see [37–40]. The forward Kolmogorov equation for the density of states F is obtained in the same manner as in [33]: we multiply (17) by F , integrate over \mathbf{X} and \mathbf{V} , change the variable of integration in the first term of the collision integral from $C_{ij}(\mathbf{V})$ to \mathbf{V} , and then strip the integral together with ψ , while making use of (11), and the fact that the Jacobian of C_{ij} is unity. The resulting forward Kolmogorov equation is given via

$$\frac{\partial F}{\partial t} + \mathbf{V} \cdot \frac{\partial F}{\partial \mathbf{X}} = \frac{\partial \Phi}{\partial \mathbf{X}} \cdot \frac{\partial F}{\partial \mathbf{V}} + \sum_{i=1}^{K-1} \sum_{j=i+1}^K \lambda_{ij} [F(C_{ij}^{-1}(\mathbf{V})) - F(\mathbf{V})]. \quad (18)$$

It is easy to find some steady states of (18) if we require that F is invariant under collisions, that is,

$$F(C_{ij}(\mathbf{V})) = F(\mathbf{V}), \quad (19)$$

for all pairs of molecules. For such F , the forward Kolmogorov equation (18) becomes

$$\frac{\partial F}{\partial t} + \mathbf{V} \cdot \frac{\partial F}{\partial \mathbf{X}} = \frac{\partial \Phi}{\partial \mathbf{X}} \cdot \frac{\partial F}{\partial \mathbf{V}}. \quad (20)$$

Next, we note that $F = F_0(E)$ satisfies (19) (since the energy is invariant under the collisions), and is at the same time the steady state for (20), which means that it is automatically the steady state for the forward Kolmogorov equation (18). Among all such states, the canonical Gibbs state is given via

$$F_G = \frac{1}{(2\pi\theta_0)^{KN/2} Z_K \Omega^K} \exp\left(-\frac{\|\mathbf{V}\|^2 + 2\Phi(\mathbf{X})}{2\theta_0}\right), \quad Z_K = \int e^{-\Phi/\theta_0} d\mathbf{x}_1 \dots d\mathbf{x}_K, \quad (21)$$

where Ω is the full solid angle of the domain of rotational coordinates, and θ_0 is the equilibrium kinetic temperature of the system of molecules. Here, observe that, thanks to (10) and (11), the presence of stochastic rotational collisions does not affect the structure of the steady state; this is to the contrary of what we had previously in [33], where the asymmetry of the intensity of collisions created the “potential well” instead.

A solution of the forward Kolmogorov equation (18) possesses the following entropy inequalities:

$$-\frac{\partial}{\partial t} \int F \ln F d\mathbf{X} d\mathbf{V} \geq 0, \quad \frac{\partial}{\partial t} \int F \ln\left(\frac{F}{F_0}\right) d\mathbf{X} d\mathbf{V} \leq 0, \quad (22)$$

where F_0 is a steady state of (18). Above, the first quantity is the Shannon entropy [41], while the second one is the Kullback-Leibler entropy [42]. The proof of the relations in (22) is given in Appendix A.

B. Structure of a two-molecule marginal distribution of the Gibbs state

Let us integrate F_G over all molecules but the first two. This integration decomposes into the product of integrals over the velocities and coordinates separately:

$$F_G^{(2)} = \frac{1}{(2\pi\theta_0)^N \Omega^2} e^{-\langle (\|\mathbf{v}_1\|^2 + \|\mathbf{w}_1\|^2 + \|\mathbf{v}_2\|^2 + \|\mathbf{w}_2\|^2) / 2\theta_0 \rangle} \frac{1}{Z_K} \int e^{-\Phi/\theta_0} d\mathbf{x}_3 \dots d\mathbf{x}_K. \quad (23)$$

Next, note that the single-particle marginal distribution f_G is given via

$$f_G(\mathbf{v}, \mathbf{w}) = \frac{1}{(2\pi\theta_0)^{N/2} V \Omega} e^{-\langle (\|\mathbf{v}\|^2 + \|\mathbf{w}\|^2) / 2\theta_0 \rangle}, \quad (24)$$

where V is the volume of the domain of translational coordinates. The reason for the form above is that, spatially, F_G depends only on the differences of the translational coordinates, and thus the integration over all molecules but one removes the spatial dependence completely. Thus, in terms of f_G , $F_G^{(2)}$ can be written in the form

$$F_G^{(2)} = f_G(\mathbf{v}_1, \mathbf{w}_1) f_G(\mathbf{v}_2, \mathbf{w}_2) \frac{V^2}{Z_K} \int e^{-\Phi/\theta_0} d\mathbf{x}_3 \dots d\mathbf{x}_K. \quad (25)$$

Next, let us look at the factor which multiplies the product of f_G 's. It can be written in the form

$$\frac{V^2}{Z_K} \int e^{-\Phi/\theta_0} d\mathbf{x}_3 \dots d\mathbf{x}_K = \frac{K}{K-1} e^{-\phi(\|\mathbf{x}_1 - \mathbf{x}_2\|)/\theta_0} Y_K(\theta_0, \|\mathbf{x}_1 - \mathbf{x}_2\|), \quad (26)$$

where $Y_K(\theta_0, r)$ is the pair cavity distribution function for K molecules [43,44]:

$$Y_K(\theta_0, \|\mathbf{x}_1 - \mathbf{x}_2\|) = \frac{K-1}{K} \frac{V^2}{Z_K} \int \prod_{i=3}^K e^{-[\phi(\|\mathbf{x}_1 - \mathbf{x}_i\|) + \phi(\|\mathbf{x}_2 - \mathbf{x}_i\|)]/\theta_0} \prod_{j=i+1}^K e^{-\phi(\|\mathbf{x}_i - \mathbf{x}_j\|)/\theta_0} d\mathbf{x}_3 \dots d\mathbf{x}_K. \quad (27)$$

Thus, with help of $Y_K(\theta_0, r)$, $F_G^{(2)}$ is given via

$$F_G^{(2)} = \frac{K}{K-1} e^{-\phi(\|\mathbf{x}_1 - \mathbf{x}_2\|)/\theta_0} Y_K(\theta_0, \|\mathbf{x}_1 - \mathbf{x}_2\|) f_G(\mathbf{v}_1, \mathbf{w}_1) f_G(\mathbf{v}_2, \mathbf{w}_2). \quad (28)$$

IV. EQUATION FOR THE DISTRIBUTION OF A SINGLE MOLECULE

Let us integrate the forward Kolmogorov equation (18) over all molecules but the first one, and, for convenience, denote $\mathbf{z}_i = (\mathbf{x}_i, \mathbf{y}_i, \mathbf{v}_i, \mathbf{w}_i)$:

$$\begin{aligned} \frac{\partial f}{\partial t} + \mathbf{v} \cdot \frac{\partial f}{\partial \mathbf{x}} + \mathbf{w} \cdot \frac{\partial f}{\partial \mathbf{y}} &= \sum_{i=2}^K \int \left(\frac{\partial}{\partial \mathbf{x}} \phi(\|\mathbf{x} - \mathbf{x}_i\|) \cdot \frac{\partial F_{1,i}^{(2)}(\mathbf{z}, \mathbf{z}_i)}{\partial \mathbf{v}} \right. \\ &\quad \left. + \lambda_{1i} [F_{1,i}^{(2)}(C^{-1}(\mathbf{z}, \mathbf{z}_i)) - F_{1,i}^{(2)}(\mathbf{z}, \mathbf{z}_i)] \right) d\mathbf{z}_i. \end{aligned} \quad (29)$$

This equation constitutes the first iteration of the Bogoliubov-Born-Green-Kirkwood-Yvon [26–28] hierarchy (BBGKY). In order to obtain a closure for the right-hand side of (29) in terms of f , as previously in [24,25,33], we assume that all pair distributions $F_{1,i}^{(2)}$ are identical, which leads to

$$\begin{aligned} \frac{\partial f}{\partial t} + \mathbf{v} \cdot \frac{\partial f}{\partial \mathbf{x}} + \mathbf{w} \cdot \frac{\partial f}{\partial \mathbf{y}} &= (K-1) \int \left(\frac{\partial}{\partial \mathbf{x}} \phi(\|\mathbf{x} - \mathbf{x}_2\|) \cdot \frac{\partial F^{(2)}(\mathbf{z}, \mathbf{z}_2)}{\partial \mathbf{v}} \right. \\ &\quad \left. + \lambda_{12} [F^{(2)}(C^{-1}(\mathbf{z}, \mathbf{z}_2)) - F^{(2)}(\mathbf{z}, \mathbf{z}_2)] \right) d\mathbf{z}_2. \end{aligned} \quad (30)$$

This is a standard assumption in kinetic theory [45], whose purpose is a formal reduction of the multimolecular dynamics to those of a single molecule, and, therefore, we use it here for the lack of a better option. However, one must understand that, in practice, such an assumption can only hold for a relatively small “parcel” of gas (confined, for example, to a periodic cube whose size is not much larger than the mean-free path), otherwise there would be no reason for different pairs of molecules to have identical distributions. As a result, a kinetic interaction of such a parcel with surroundings is not accounted for in the context of such a formalism, which below leads to an empirical closure of the moment hierarchy in an attempt to accommodate such unaccounted interactions.

Next, we need to approximate $F^{(2)}$ in terms of f ; as we have done previously in [24,33], we assume that $F^{(2)}$ has the same form as does $F_G^{(2)}$ in (28):

$$F^{(2)}(\mathbf{z}, \mathbf{z}_2) = \frac{K}{K-1} e^{-\phi(\|\mathbf{x}-\mathbf{x}_2\|)/\theta} Y_K(\theta, \|\mathbf{x}-\mathbf{x}_2\|) f(\mathbf{z}) f(\mathbf{z}_2). \quad (31)$$

Above, θ is no longer an equilibrium temperature; instead, it is now the average kinetic energy of the given molecule (and thus an appropriate moment of f itself), which endows it with a dependence on \mathbf{x} . Thus, for symmetry, in the closure above we compute θ at the midpoint between \mathbf{x} and \mathbf{x}_2 : $\theta = \theta[(\mathbf{x} + \mathbf{x}_2)/2]$. In addition, we renormalize f so that it is the mass density $f \rightarrow Km f$, where m is the mass of a single molecule. Applying the closure and the rescaling, we arrive at the following closed equation:

$$\begin{aligned} \frac{\partial f}{\partial t} + \mathbf{v} \cdot \frac{\partial f}{\partial \mathbf{x}} + \mathbf{w} \cdot \frac{\partial f}{\partial \mathbf{y}} &= \frac{1}{m} \int e^{-\phi(\|\mathbf{x}-\mathbf{x}_2\|)/\theta[(\mathbf{x}+\mathbf{x}_2)/2]} Y_K(\theta[(\mathbf{x}+\mathbf{x}_2)/2], \|\mathbf{x}-\mathbf{x}_2\|) \\ &\times \left(\frac{\partial}{\partial \mathbf{x}} \phi(\|\mathbf{x}-\mathbf{x}_2\|) \cdot \frac{\partial f(\mathbf{z})}{\partial \mathbf{v}} f(\mathbf{z}_2) + \lambda(\mathbf{z}-\mathbf{z}_2) [f(\mathbf{z}'') f(\mathbf{z}_2'') - f(\mathbf{z}) f(\mathbf{z}_2)] \right) d\mathbf{z}_2, \end{aligned} \quad (32)$$

where \mathbf{z}'' and \mathbf{z}_2'' refer to the inverse of the collision mapping, $(\mathbf{z}'', \mathbf{z}_2'') = C^{-1}(\mathbf{z}, \mathbf{z}_2)$. Above, the kinetic temperature θ is given as follows: let us introduce the average $\langle \psi \rangle$ of a function $\psi(\mathbf{x}, \mathbf{y}, \mathbf{v}, \mathbf{w})$ via

$$\langle \psi \rangle(t, \mathbf{x}) = \int \psi(\mathbf{x}, \mathbf{y}, \mathbf{v}, \mathbf{w}) f(t, \mathbf{x}, \mathbf{y}, \mathbf{v}, \mathbf{w}) d\mathbf{y} d\mathbf{v} d\mathbf{w}. \quad (33)$$

Then, we define the density ρ , linear and angular velocities \mathbf{u} and \mathbf{u}_w , respectively, and the kinetic temperature θ via the following velocity moments:

$$\rho = \langle 1 \rangle, \quad \rho \mathbf{u} = \langle \mathbf{v} \rangle, \quad \rho \mathbf{u}_w = \langle \mathbf{w} \rangle, \quad \rho \theta = \frac{1}{N} \langle \|\mathbf{v} - \mathbf{u}\|^2 + \|\mathbf{w} - \mathbf{u}_w\|^2 \rangle. \quad (34)$$

Above, the product $\rho \theta$ can be referred to as the “kinetic” pressure, defined through the equation of state for an ideal gas, as opposed to the “true” van der Waals’ pressure, to be found below. With the above notations, we can separate the integrals in (32) as follows:

$$\begin{aligned} \frac{\partial f}{\partial t} + \mathbf{v} \cdot \frac{\partial f}{\partial \mathbf{x}} + \mathbf{w} \cdot \frac{\partial f}{\partial \mathbf{y}} &= \frac{\partial f(\mathbf{z})}{\partial \mathbf{v}} \cdot \frac{1}{m} \int e^{-\frac{\phi(\|\mathbf{x}-\mathbf{x}_2\|)}{\theta[(\mathbf{x}+\mathbf{x}_2)/2]}} Y_K(\theta[(\mathbf{x}+\mathbf{x}_2)/2], \|\mathbf{x}-\mathbf{x}_2\|) \\ &\times \frac{\partial}{\partial \mathbf{x}} \phi(\|\mathbf{x}-\mathbf{x}_2\|) \rho(\mathbf{x}_2) d\mathbf{x}_2 + \frac{1}{m} \int e^{-\frac{\phi(\|\mathbf{x}-\mathbf{x}_2\|)}{\theta[(\mathbf{x}+\mathbf{x}_2)/2]}} Y_K(\theta[(\mathbf{x}+\mathbf{x}_2)/2], \|\mathbf{x}-\mathbf{x}_2\|) \\ &\times \lambda(\mathbf{z}-\mathbf{z}_2) [f(\mathbf{z}'') f(\mathbf{z}_2'') - f(\mathbf{z}) f(\mathbf{z}_2)] d\mathbf{z}_2. \end{aligned} \quad (35)$$

A. Hydrodynamic limit

For most practical situations, the size of each molecule is much smaller than the size of the domain. If so, the transport equation for f can be simplified further by computing what is known as the “hydrodynamic limit,” that is, an appropriate limit where the size of a molecule becomes

infinitely small in comparison with the size of the domain. To this end, we introduce the constant parameter σ , which is to be the ‘‘diameter’’ of a molecule, and, with its help, rescale the distance between the molecules in all of the properties of molecular interactions:

$$\phi(r) \rightarrow \phi(r/\sigma), \quad Y_K(\theta, r) \rightarrow Y_K(\theta, r/\sigma), \quad \lambda(\mathbf{x}, \mathbf{y}, \mathbf{v}, \mathbf{w}) \rightarrow \lambda(\mathbf{x}/\sigma, \mathbf{y}, \mathbf{v}, \mathbf{w}), \quad (36a)$$

$$\mathbf{g}(\mathbf{x}, \mathbf{y}, \mathbf{v}, \mathbf{w}) \rightarrow \mathbf{g}(\mathbf{x}/\sigma, \mathbf{y}, \mathbf{v}, \mathbf{w}), \quad \mathbf{h}(\mathbf{x}, \mathbf{y}, \mathbf{v}, \mathbf{w}) \rightarrow \mathbf{h}(\mathbf{x}/\sigma, \mathbf{y}, \mathbf{v}, \mathbf{w}). \quad (36b)$$

Then, as $\sigma \rightarrow 0$, $m \rightarrow 0$, and $K \rightarrow \infty$, with m/σ^3 and Km being constants (so that the density of a molecule and the total mass of the system would be fixed), Eq. (35) is transformed as follows:

$$\frac{\partial f}{\partial t} + \mathbf{v} \cdot \frac{\partial f}{\partial \mathbf{x}} + \mathbf{w} \cdot \frac{\partial f}{\partial \mathbf{y}} = \frac{1}{\rho} \frac{\partial \bar{\phi}}{\partial \mathbf{x}} \cdot \frac{\partial f}{\partial \mathbf{v}} + \mathcal{C}(f). \quad (37)$$

Above, the potential forcing and the collision integral in the right-hand side are given, respectively, via

$$\bar{\phi} = \frac{2\pi}{3} \frac{\sigma^3}{m} \rho^2(\mathbf{x}) \theta(\mathbf{x}) \int_0^\infty (1 - e^{-\phi(r)/\theta(\mathbf{x})}) \frac{\partial}{\partial r} (r^3 Y(\theta(\mathbf{x}), r)) dr, \quad (38a)$$

$$\begin{aligned} \mathcal{C}(f) = & \frac{\sigma^3}{m} \int \alpha(\mathbf{x}, \mathbf{r}, \mathbf{y} - \mathbf{y}_2, \mathbf{v} - \mathbf{v}_2, \mathbf{w} - \mathbf{w}_2) [f(\mathbf{x}, \mathbf{y}, \mathbf{v}'', \mathbf{w}'') f(\mathbf{x}, \mathbf{y}_2, \mathbf{v}_2'', \mathbf{w}_2'') \\ & - f(\mathbf{x}, \mathbf{y}, \mathbf{v}, \mathbf{w}) f(\mathbf{x}, \mathbf{y}_2, \mathbf{v}_2, \mathbf{w}_2)] d\mathbf{r} d\mathbf{y}_2 d\mathbf{v}_2 d\mathbf{w}_2, \end{aligned} \quad (38b)$$

$$\alpha(\mathbf{x}, \mathbf{r}, \mathbf{y}, \mathbf{v}, \mathbf{w}) = \lambda(\mathbf{r}, \mathbf{y}, \mathbf{v}, \mathbf{w}) e^{-\phi(\|\mathbf{r}\|)/\theta(\mathbf{x})} Y(\theta(\mathbf{x}), \|\mathbf{r}\|), \quad (38c)$$

where the integration in $d\mathbf{r}$ occurs over \mathbb{R}^3 . Below, we refer to (37) as the *Boltzmann-Vlasov equation* because it contains both the deterministic potential (as in the Vlasov equation [29]), and the stochastic collision integral (as in the Boltzmann equation [46]).

In (38), $Y(\theta, r)$ denotes the cavity distribution function for infinitely many molecules, and the increments in the collision mapping C are computed as

$$\mathbf{g}_{12} = \mathbf{g}(\mathbf{r}, \mathbf{y}_1 - \mathbf{y}_2, \mathbf{v}_1 - \mathbf{v}_2, \mathbf{w}_1 - \mathbf{w}_2), \quad (39a)$$

$$\mathbf{h}_{12} = \mathbf{h}(\mathbf{r}, \mathbf{y}_1 - \mathbf{y}_2, \mathbf{v}_1 - \mathbf{v}_2, \mathbf{w}_1 - \mathbf{w}_2). \quad (39b)$$

The derivation of the forcing and collision terms in (38) is presented in Appendix B. Since it is assumed that the volume of the domain is constant, we can see that the packing fraction (that is, the total volume of molecules divided by the volume of the domain) also approaches a constant, and, in particular, does not vanish in the hydrodynamic limit:

$$K\sigma^3 \cdot \frac{1}{V} = (Km) \frac{\sigma^3}{m} \frac{1}{V} \sim \text{const.} \quad (40)$$

Generally, the cavity distribution function $Y(\theta, r)$ also depends on the packing fraction.

B. Steady state of the collision integral

Observe that, irrespectively of α , the collision integral in (38b) is guaranteed to be zero when

$$f(\mathbf{x}, \mathbf{y}, \mathbf{v}'', \mathbf{w}'') f(\mathbf{x}, \mathbf{y}_2, \mathbf{v}_2'', \mathbf{w}_2'') = f(\mathbf{x}, \mathbf{y}, \mathbf{v}, \mathbf{w}) f(\mathbf{x}, \mathbf{y}_2, \mathbf{v}_2, \mathbf{w}_2) \quad (41)$$

or, if we take a logarithm on both sides,

$$\ln f(\mathbf{x}, \mathbf{y}, \mathbf{v}'', \mathbf{w}'') + \ln f(\mathbf{x}, \mathbf{y}_2, \mathbf{v}_2'', \mathbf{w}_2'') = \ln f(\mathbf{x}, \mathbf{y}, \mathbf{v}, \mathbf{w}) + \ln f(\mathbf{x}, \mathbf{y}_2, \mathbf{v}_2, \mathbf{w}_2). \quad (42)$$

Taking into account the momentum and kinetic energy conservation laws of collision (3), we conclude that the above identity holds under the same conditions as in the usual Boltzmann equation [45–48], that is,

$$\ln f = a_1 + \mathbf{a}_2 \cdot \mathbf{v} + \mathbf{a}_3 \cdot \mathbf{w} + a_4 (\|\mathbf{v}\|^2 + \|\mathbf{w}\|^2), \quad (43)$$

for arbitrary a_1, a_2, a_3 , and a_4 . As a result, the Maxwell-Boltzmann equilibrium state

$$f_{\text{MB}} = \frac{\rho}{(2\pi\theta)^{N/2}} \exp\left(-\frac{\|\mathbf{v} - \mathbf{u}\|^2 + \|\mathbf{w} - \mathbf{u}_w\|^2}{2\theta}\right), \quad (44)$$

which has the correct values of the moments in (34), is a steady state for the collision integral alone. Additionally, if $\rho, \mathbf{u}, \mathbf{u}_w$, and θ do not depend on \mathbf{x} , then f_{MB} becomes a steady state for the whole Boltzmann-Vlasov equation in (37).

C. Moments of the collision integral

We define a moment of the collision integral via

$$\begin{aligned} \langle \psi \rangle_{\mathcal{C}}(t, \mathbf{x}) &= \int \psi(\mathbf{x}, \mathbf{y}, \mathbf{v}, \mathbf{w}) \mathcal{C}(f) d\mathbf{y} d\mathbf{v} d\mathbf{w} = \int \alpha(\mathbf{x}, \mathbf{r}, \mathbf{y} - \mathbf{y}_2, \mathbf{v} - \mathbf{v}_2, \mathbf{w} - \mathbf{w}_2) \\ &\quad \times [\psi(\mathbf{x}, \mathbf{y}, \mathbf{v}', \mathbf{w}') - \psi(\mathbf{x}, \mathbf{y}, \mathbf{v}, \mathbf{w})] f(\mathbf{x}, \mathbf{y}, \mathbf{v}, \mathbf{w}) \\ &\quad \times f(\mathbf{x}, \mathbf{y}_2, \mathbf{v}_2, \mathbf{w}_2) d\mathbf{r} d\mathbf{y}_2 d\mathbf{v}_2 d\mathbf{w}_2 d\mathbf{y} d\mathbf{v} d\mathbf{w}, \end{aligned} \quad (45)$$

where in the second identity we changed the collision mapping from backward to forward under the integral. Observe that, due to (11), $\langle \psi \rangle_{\mathcal{C}}$ is invariant under the permutation of the two molecules:

$$\begin{aligned} \langle \psi \rangle_{\mathcal{C}}(t, \mathbf{x}) &= \frac{1}{2} \int \alpha(\mathbf{x}, \mathbf{r}, \mathbf{y} - \mathbf{y}_2, \mathbf{v} - \mathbf{v}_2, \mathbf{w} - \mathbf{w}_2) [\psi(\mathbf{x}, \mathbf{y}, \mathbf{v}', \mathbf{w}') + \psi(\mathbf{x}, \mathbf{y}_2, \mathbf{v}'_2, \mathbf{w}'_2) \\ &\quad - \psi(\mathbf{x}, \mathbf{y}, \mathbf{v}, \mathbf{w}) - \psi(\mathbf{x}, \mathbf{y}_2, \mathbf{v}_2, \mathbf{w}_2)] f(\mathbf{x}, \mathbf{y}, \mathbf{v}, \mathbf{w}) \\ &\quad \times f(\mathbf{x}, \mathbf{y}_2, \mathbf{v}_2, \mathbf{w}_2) d\mathbf{r} d\mathbf{y}_2 d\mathbf{v}_2 d\mathbf{w}_2 d\mathbf{y} d\mathbf{v} d\mathbf{w}. \end{aligned} \quad (46)$$

Due to the momentum and kinetic energy conservation laws of the collision mechanics, we can see that the collision moments are zero for $\psi = 1, \mathbf{v}, \mathbf{w}, (\|\mathbf{v}\|^2 + \|\mathbf{w}\|^2)$, and, subsequently, $\ln f_{\text{MB}}$. Additionally, we show in Appendix C that

$$\langle \ln f \rangle_{\mathcal{C}} \leq 0. \quad (47)$$

Then, it is easy to verify that the following inequalities hold for the Shannon entropy $\langle -\ln f \rangle$ and the Kullback-Leibler entropy $\langle \ln(f/f_{\text{MB}}) \rangle$:

$$\frac{\partial}{\partial t} \langle -\ln f \rangle + \nabla_{\mathbf{x}} \cdot \langle -\mathbf{v} \ln f \rangle \geq 0, \quad \frac{\partial}{\partial t} \langle \ln(f/f_{\text{MB}}) \rangle + \nabla_{\mathbf{x}} \cdot \langle \mathbf{v} \ln(f/f_{\text{MB}}) \rangle \leq 0. \quad (48)$$

The first inequality constitutes Boltzmann's H theorem for (37).

D. Velocity moment equations

To obtain the transport equation for a velocity moment of the form (33), we integrate the Boltzmann-Vlasov equation in (37) against $\psi(\mathbf{v}, \mathbf{w})$, and assume that there are no boundary effects when the forcing is integrated by parts:

$$\frac{\partial \langle \psi \rangle}{\partial t} + \nabla \cdot \langle \psi \mathbf{v} \rangle = -\frac{1}{\rho} \nabla \bar{\phi} \cdot \langle \nabla_{\mathbf{v}} \psi \rangle + \langle \psi \rangle_{\mathcal{C}}. \quad (49)$$

Above, “ ∇ ” without a subscript denotes the differentiation in \mathbf{x} . From (3) and (46), it automatically follows that, for $\psi = 1, \mathbf{v}, \mathbf{w}$ and $(\|\mathbf{v}\|^2 + \|\mathbf{w}\|^2)$, the collision integral disappears. In particular, the transport equation for the density ρ is given via

$$\frac{\partial \langle 1 \rangle}{\partial t} + \nabla \cdot \langle \mathbf{v} \rangle = 0 \quad \text{or} \quad \frac{\partial \rho}{\partial t} + \nabla \cdot (\rho \mathbf{u}) = 0, \quad (50)$$

where we recall the notations in (34). For the momentum transport equation, we write

$$\frac{\partial \langle \mathbf{v} \rangle}{\partial t} + \nabla \cdot \langle \mathbf{v}^2 \rangle = -\nabla \bar{\phi}, \quad \frac{\partial \langle \mathbf{w} \rangle}{\partial t} + \nabla \cdot \langle \mathbf{w} \mathbf{v}^T \rangle = \mathbf{0}, \quad (51)$$

where we adopt the convention that the tensor contraction occurs over the trailing (or column) index. Introducing the stresses

$$\mathbf{S} = \langle (\mathbf{v} - \mathbf{u})^2 \rangle - \rho \theta \mathbf{I}, \quad \langle (\mathbf{v} - \mathbf{u})(\mathbf{w} - \mathbf{u}_w)^T \rangle = \mathbf{S}_{vw}, \quad (52)$$

we write the equations for the linear and angular momenta above as

$$\frac{\partial(\rho \mathbf{u})}{\partial t} + \nabla \cdot [\rho(\mathbf{u}^2 + \theta \mathbf{I}) + \mathbf{S}] = -\nabla \bar{\phi}, \quad \frac{\partial(\rho \mathbf{u}_w)}{\partial t} + \nabla \cdot (\rho \mathbf{u}_w \mathbf{u}^T + \mathbf{S}_{vw}) = \mathbf{0}. \quad (53)$$

For the energy transport equation, we write

$$\frac{\partial}{\partial t} \langle \|\mathbf{v}\|^2 + \|\mathbf{w}\|^2 \rangle + \nabla \cdot \langle (\|\mathbf{v}\|^2 + \|\mathbf{w}\|^2) \mathbf{v} \rangle = \frac{1}{\rho} \langle (\|\mathbf{v}\|^2 + \|\mathbf{w}\|^2) \nabla_v \cdot (f \nabla_x \bar{\phi}) \rangle. \quad (54)$$

Introducing the heat flux

$$\mathbf{q} = \frac{1}{2} \langle (\|\mathbf{v} - \mathbf{u}\|^2 + \|\mathbf{w} - \mathbf{u}_w\|^2) (\mathbf{v} - \mathbf{u}) \rangle, \quad (55)$$

we observe, via simple manipulations, that

$$\langle \|\mathbf{v}\|^2 + \|\mathbf{w}\|^2 \rangle = \rho (\|\mathbf{u}\|^2 + \|\mathbf{u}_w\|^2 + N\theta), \quad (56a)$$

$$\langle (\|\mathbf{v}\|^2 + \|\mathbf{w}\|^2) \mathbf{v} \rangle = \rho [\|\mathbf{u}\|^2 + \|\mathbf{u}_w\|^2 + (N+2)\theta] \mathbf{u} + 2(\mathbf{S} \mathbf{u} + \mathbf{S}_{vw} \mathbf{u}_w + \mathbf{q}), \quad (56b)$$

$$\frac{1}{\rho} \langle (\|\mathbf{v}\|^2 + \|\mathbf{w}\|^2) \nabla_v \cdot (f \nabla_x \bar{\phi}) \rangle = -2\mathbf{u} \cdot \nabla \bar{\phi}, \quad (56c)$$

which leads to

$$\begin{aligned} \frac{\partial}{\partial t} [\rho (\|\mathbf{u}\|^2 + \|\mathbf{u}_w\|^2 + N\theta)] + \nabla \cdot [\rho (\|\mathbf{u}\|^2 + \|\mathbf{u}_w\|^2 + (N+2)\theta) \mathbf{u} \\ + 2(\mathbf{S} \mathbf{u} + \mathbf{S}_{vw} \mathbf{u}_w + \mathbf{q})] = -2\mathbf{u} \cdot \nabla \bar{\phi}. \end{aligned} \quad (57)$$

In order to obtain the equation for the kinetic pressure $\rho\theta$, we express the time derivatives via

$$\begin{aligned} \frac{\partial(\rho \|\mathbf{u}\|^2)}{\partial t} &= 2\mathbf{u} \cdot \frac{\partial(\rho \mathbf{u})}{\partial t} - \|\mathbf{u}\|^2 \frac{\partial \rho}{\partial t} = \|\mathbf{u}\|^2 \nabla \cdot (\rho \mathbf{u}) - 2\mathbf{u}^T \nabla \cdot [\rho \mathbf{u}^2 + (\rho\theta + \bar{\phi}) \mathbf{I} + \mathbf{S}] \\ &= -\nabla \cdot (\rho \|\mathbf{u}\|^2 \mathbf{u}) - 2\mathbf{u} \cdot \nabla (\rho\theta + \bar{\phi}) - 2\mathbf{u}^T \nabla \cdot \mathbf{S}, \end{aligned} \quad (58a)$$

$$\begin{aligned} \frac{\partial(\rho \|\mathbf{u}_w\|^2)}{\partial t} &= 2\mathbf{u}_w \cdot \frac{\partial(\rho \mathbf{u}_w)}{\partial t} - \|\mathbf{u}_w\|^2 \frac{\partial \rho}{\partial t} = \|\mathbf{u}_w\|^2 \nabla \cdot (\rho \mathbf{u}_w) - 2\mathbf{u}_w^T \nabla \cdot (\rho \mathbf{u}_w \mathbf{u}_w + \mathbf{S}_{vw}) \\ &= -\nabla \cdot (\rho \|\mathbf{u}_w\|^2 \mathbf{u}_w) - 2\mathbf{u}_w^T \nabla \cdot \mathbf{S}_{vw}, \end{aligned} \quad (58b)$$

and subtract from the energy transport equation, which, upon division by N , retains the time derivative for the kinetic pressure only:

$$\frac{\partial(\rho\theta)}{\partial t} + \nabla \cdot (\rho\theta \mathbf{u}) + \frac{2}{N} (\rho\theta \nabla \cdot \mathbf{u} + \mathbf{S} : \nabla \mathbf{u} + \mathbf{S}_{vw} : \nabla \mathbf{u}_w + \nabla \cdot \mathbf{q}) = 0. \quad (59)$$

V. A CLOSURE FOR THE HEAT FLUX BASED ON A PRESCRIBED SPECIFIC-HEAT CAPACITY

The Boltzmann-Vlasov equation (37) and, subsequently, the transport equations for the density (50), momentum (53), and pressure (59) are derived from the multimolecular forward Kolmogorov equation (18), under the assumption that the latter represents a closed system of molecules, which has no interaction with any outside effects. Moreover, all molecules are regarded to be statistically

identical and thus any molecule is equally likely to collide with any other molecule, which of course, cannot be true for domains whose size exceeds the length of the mean-free path by many orders of magnitude. As a result, the Boltzmann-Vlasov equation practically describes the behavior of a small parcel of gas, which does not interact with its surroundings at all.

Subsequently, its direct and naive closure, which solely relies upon, broadly speaking, hypoelliptic properties of the collision integral, invariably leads to the compressible Enskog-Euler equations [33,49], where the stress and heat flux are suppressed toward zero by the collision damping, which emerges from the Chapman-Enskog expansion [34,47,48]. The Enskog-Euler equations describe a thermodynamic process, where a parcel of gas, following its trajectory, does not exchange the heat energy with the neighboring parcels at all. This is a good approximation for the behavior of a gas at short spatial and temporal scales, such as shock transitions at supersonic Mach numbers, or acoustic waves.

However, at longer temporal and spatial scales, the parcel of gas exchanges the heat energy with neighboring parcels, which results in a qualitatively different behavior such as, for example, incompressible flow, which has a tendency to manifest at subsonic Mach numbers. Furthermore, in our recent works [24,25], we demonstrated that turbulent behavior in a monatomic gas is observed for a constant-pressure (or inertial) flow. It is, however, common for the exchange of momentum to be negligible in practical situations since high Reynolds number flows are ubiquitous in nature at macroscopic scales.

Therefore, in order to arrive at a suitable closure, which realistically describes a turbulent flow regime, we assume that, while the stress is negligible as a result of the high Reynolds number condition, the heat flux is not [even despite the presence of the collision damping in (37)], since the gas exchanges the heat energy with its surroundings. To this end, we remove the terms with stresses \mathbf{S} and \mathbf{S}_{vw} from (53) and (59) to signify the high Reynolds number flow, but retain the divergence of the heat flux $\nabla \cdot \mathbf{q}$ in the pressure equation (59). Once the stresses \mathbf{S} and \mathbf{S}_{vw} are removed, the pressure equation (59) becomes decoupled from \mathbf{u}_w and \mathbf{S}_{vw} , and we can discard the equation for the angular momentum in (53) from consideration. For reasons which will become clear below, we also recall the formula for the dimensionless specific-heat capacity c_v of an ideal gas at a constant volume,

$$c_v = \frac{N}{2}, \quad (60)$$

and express N via c_v in the pressure equation (59). In the formula for c_v above, it is assumed that the kinetic energy of the gas is distributed uniformly across all of its degrees of freedom, both translational and rotational.

The above manipulations lead to the following system of transport equations for the density (50), momentum (53), and kinetic pressure (59) at a high Reynolds number:

$$\frac{\partial \rho}{\partial t} + \nabla \cdot (\rho \mathbf{u}) = 0, \quad \frac{\partial (\rho \mathbf{u})}{\partial t} + \nabla \cdot (\rho \mathbf{u}^2) + \nabla (\rho \theta + \bar{\phi}) = \mathbf{0}, \quad (61a)$$

$$\frac{\partial (\rho \theta)}{\partial t} + \nabla \cdot (\rho \theta \mathbf{u}) + \frac{1}{c_v} (\rho \theta \nabla \cdot \mathbf{u} + \nabla \cdot \mathbf{q}) = 0. \quad (61b)$$

Above, observe that the expression $\rho \theta + \bar{\phi}$ has the meaning of the “true,” or van der Waals, pressure, that is, the quantity whose gradient constitutes the forcing in the momentum equation of the gas and thereby accelerates its flow.

Although the transport equations in (61) no longer contain the stress, the divergence of the heat flux $\nabla \cdot \mathbf{q}$ is still present in the pressure equation (61b) due to yet unspecified properties of the heat exchange with the surrounding gas. Thus, we need a closure for the divergence of the heat flux.

Here, we show that the closure for $\nabla \cdot \mathbf{q}$ can be achieved if one requires the flow to have a prescribed constant specific-heat capacity c . Of course, we have to understand that one cannot simply set the specific-heat capacity to an arbitrary constant value and expect meaningful results;

yet, it is known that, for certain values of c , valid thermodynamic processes do indeed exist. For the purposes of the derivation, however, we will assume that c is an arbitrary constant parameter.

First, we multiply the whole kinetic pressure equation (61b) by a constant c :

$$\frac{\partial(c\rho\theta)}{\partial t} + \nabla \cdot (c\rho\theta\mathbf{u}) + \frac{c}{c_v}(\rho\theta\nabla \cdot \mathbf{u} + \nabla \cdot \mathbf{q}) = 0. \quad (62)$$

Next, we assume that the whole term, multiplied by c/c_v , is by itself equal to $\nabla \cdot \mathbf{q}$:

$$\frac{c}{c_v}(\rho\theta\nabla \cdot \mathbf{u} + \nabla \cdot \mathbf{q}) = \nabla \cdot \mathbf{q} \quad \text{or} \quad \nabla \cdot \mathbf{q} = \frac{c}{c_v - c} \rho\theta\nabla \cdot \mathbf{u}. \quad (63)$$

If so, (62) becomes

$$\frac{\partial(c\rho\theta)}{\partial t} + \nabla \cdot (c\rho\theta\mathbf{u} + \mathbf{q}) = 0 \quad \text{or} \quad \frac{\partial}{\partial t} \int_V c\rho\theta dV = \oint_S (c\rho\theta\mathbf{u} + \mathbf{q}) \cdot \mathbf{n} dS, \quad (64)$$

where V is the volume enclosed by a surface S , and we used Gauss' theorem with the inward unit normal vector \mathbf{n} . It is clear that the above equation describes a process with the constant specific-heat capacity equal to c ; indeed, the rate of increase of the heat energy in the volume V is the sum of the inward advective and thermal heat fluxes.

If we assume that, for a prescribed constant specific-heat capacity c , the corresponding thermodynamic process indeed exists, then the relation in (63) can be used for the heat-flux closure. Expressing $\nabla \cdot \mathbf{q}$ via $\rho\theta\nabla \cdot \mathbf{u}$ by means of (63) and substituting it into the kinetic pressure equation (61b), we obtain a closed equation for the kinetic pressure:

$$\frac{\partial(\rho\theta)}{\partial t} + \nabla \cdot (\rho\theta\mathbf{u}) + \frac{\rho\theta}{c_v - c} \nabla \cdot \mathbf{u} = 0. \quad (65)$$

The system of equations, consisting of the mass and momentum transport in (61a), and the kinetic pressure transport in (65), preserves the generalized entropy \mathcal{S} of the form

$$\mathcal{S}(c) = \rho\theta^{c-c_v} \quad (66)$$

along the stream lines. Indeed, differentiating \mathcal{S} in time, and replacing the time derivatives of ρ and $\rho\theta$ with their respective advection terms from (61a) and (65), we obtain

$$\frac{\partial\mathcal{S}}{\partial t} + \mathbf{u} \cdot \nabla\mathcal{S} = 0. \quad (67)$$

For computational purposes, it is usually desirable to express a system of transport equations in the form of conservation laws. In the present setting, the mass and momentum transport equations in (61a) indeed have the conservation law form, however, the pressure transport equation (65) does not. Fortunately, the quantity $\mathcal{A}(c)$, given via

$$\mathcal{A}(c) = \theta^{c_v - c}, \quad (68)$$

has the transport equation in the form of a conservation law:

$$\frac{\partial\mathcal{A}}{\partial t} + \nabla \cdot (\mathcal{A}\mathbf{u}) = 0. \quad (69)$$

The equations in (61a), (68), and (69) constitute a closed system of the transport equations for the high Reynolds number flow of a gas with the specific-heat capacity c .

A. Notable special cases

As we mentioned above, the equations in (61a), (66), and (67) do not necessarily describe a valid process for an arbitrary specific-heat capacity c . However, there are notable special cases for certain values of c , which are empirically known to be valid thermodynamic processes. Below we list these known special cases.

(i) *Adiabatic process.* Sending $c \rightarrow 0$ requires $\nabla \cdot \mathbf{q} \rightarrow 0$ in (63) (that is, a parcel of gas does not exchange heat energy with the surroundings), which yields the compressible Enskog-Euler equations [33,49], with the entropy \mathcal{S} given via

$$\mathcal{S}(0) = \rho\theta^{-c_v}. \quad (70)$$

This regime accurately describes processes at transonic and supersonic Mach numbers, such as acoustic waves or shock transitions.

(ii) *Process at constant density.* Sending $c \rightarrow c_v$ requires $\nabla \cdot \mathbf{u} \rightarrow 0$ in (63), which leads to the incompressible Euler equations [50,51]. The quantity which is preserved along the stream lines is naturally the density ρ of the gas, that is,

$$\mathcal{S}(c_v) = \rho. \quad (71)$$

This regime describes processes at intermediate subsonic Mach numbers, such as the flow around the airfoil of a piston engine aircraft at its typical cruising speed. In classical thermodynamics, such process is described by Gay-Lussac's law.

(iii) *Process at constant temperature.* Sending $c \rightarrow \infty$ in (63) leads to the kinetic pressure equation in the same form as that for the density, which means that the quantity which is preserved along the stream lines is the kinetic temperature θ :

$$\frac{\partial\theta}{\partial t} + \mathbf{u} \cdot \nabla\theta = 0. \quad (72)$$

In classical thermodynamics, such process is described by Boyle's law.

(iv) *Process at constant kinetic pressure.* Setting $c = c_p$, where the latter is the specific-heat capacity at a constant kinetic pressure, and recalling Mayer's relation

$$c_p = c_v + 1, \quad \text{we find that} \quad \mathcal{S}(c_v + 1) = \rho\theta, \quad (73)$$

that is, the kinetic pressure is preserved along the stream lines. In classical thermodynamics, such process is described by Charles' law.

B. Suitable thermodynamic process for a turbulent gas flow at normal conditions

At this point, we need to choose one of the four thermodynamic processes above to model a turbulent flow in realistic conditions. Here, we note that, normally, turbulence is observed roughly in the same conditions as is convection in the atmosphere under the effect of gravity. Convection occurs as follows: when a parcel of air, being initially in hydrostatic balance between the gravity force and the pressure gradient, increases its temperature, it simultaneously expands. However, its pressure remains invariant; as an example, envision a hot air balloon, clearly, the pressure inside it is the same as outside. The expansion decreases the density of the parcel and upsets the hydrostatic balance, that is, the gravity force, being the product of the density and the gravity acceleration, is no longer sufficient to counter the pressure gradient. Thus, the warmer air rises up.

From what is described above, observe that only the process at constant kinetic pressure is consistent with the phenomenon of convection; otherwise, either the gas cannot increase its temperature, or it cannot expand, or, worse yet, an increase in temperature results in compression of the gas (adiabatic process). Setting $c = c_v + 1$ in (65) leads to

$$\frac{\partial(\rho\theta)}{\partial t} + \mathbf{u} \cdot \nabla(\rho\theta) = 0, \quad (74)$$

which, together with the mass and momentum transport equations in (61a), constitutes the same transport equations for a balanced flow as those in [24,25] for a monatomic gas. What is more surprising is that the equations in (61a) and (74) no longer contain the specific-heat capacity c_v and, therefore, apply to any polyatomic gas, as long as it possesses only translational and rotational

degrees of freedom. For numerical computations, we note that

$$\mathcal{A}(c_v + 1) = \theta^{-1}, \quad (75)$$

which yields the conservation laws for the transport of mass, momentum, and inverse kinetic temperature, identical to those for a monatomic gas [24,25]:

$$\frac{\partial \rho}{\partial t} + \nabla \cdot (\rho \mathbf{u}) = 0, \quad \frac{\partial(\rho \mathbf{u})}{\partial t} + \nabla \cdot (\rho \mathbf{u}^2) + \nabla(\rho \theta + \bar{\phi}) = \mathbf{0}, \quad \frac{\partial(\theta^{-1})}{\partial t} + \nabla \cdot (\theta^{-1} \mathbf{u}) = 0. \quad (76)$$

In what follows, we study the special case of balanced flow (76), where the kinetic pressure throughout the domain is constant $\rho \theta = p_0$ (also known as inertial flow). In such a case, the inverse temperature θ^{-1} becomes a constant multiple of the density ρ , which makes the equation for the former redundant. The system of equations for such a flow is thus comprised solely by the mass and momentum transport equations:

$$\frac{\partial \rho}{\partial t} + \nabla \cdot (\rho \mathbf{u}) = 0, \quad \frac{\partial(\rho \mathbf{u})}{\partial t} + \nabla \cdot (\rho \mathbf{u}^2) + \nabla \bar{\phi} = \mathbf{0}. \quad (77)$$

C. Hard-sphere approximation for the mean field potential

Following [24,25], here we approximate the mean field potential $\bar{\phi}$ in (38a) via a simple formula, which can be obtained for a hard-sphere interatomic potential. Observe that, for ϕ being that of a hard sphere, that is, zero for $r \geq 1$, and infinite for $r < 1$, the integral in (38a) becomes the cavity distribution function itself,

$$\int_0^\infty (1 - e^{-\phi_{\text{HS}}(r)/\theta}) \frac{\partial}{\partial r} (r^3 Y_{\text{HS}}(\theta, r)) dr = \int_0^1 \frac{\partial}{\partial r} (r^3 Y_{\text{HS}}(\theta, r)) dr = Y_{\text{HS}}(\theta, 1), \quad (78)$$

which leads to

$$\bar{\phi}_{\text{HS}} = \frac{2\pi}{3} \frac{\sigma^3}{m} \rho^2 \theta Y_{\text{HS}}(\theta, 1) = \frac{4\rho^2 \theta}{\rho_{\text{HS}}} Y_{\text{HS}}(\theta, 1), \quad \rho_{\text{HS}} = \frac{6m}{\pi \sigma^3}. \quad (79)$$

Here, observe that, for hard spheres, the potential forcing in the momentum equation is the same as the one in the Enskog-Euler equations [33,49], that is, the hard-sphere collision integral in the Enskog equation produces the same momentum forcing term as does the hard-sphere potential in the Boltzmann-Vlasov equation (37).

In turn, the cavity distribution function $Y_{\text{HS}}(\theta, 1)$ for hard spheres is no longer a function of the temperature, and is only a function of the packing fraction ρ/ρ_{HS} [43,44]:

$$Y_{\text{HS}}(\theta, 1) = \exp\left(\frac{5}{2} \frac{\rho}{\rho_{\text{HS}}}\right) + o\left(\frac{\rho}{\rho_{\text{HS}}}\right). \quad (80)$$

In the numerical simulations that follow, the packing fraction $\rho/\rho_{\text{HS}} \sim 10^{-3}$; in such a situation, $Y \approx 1$ and $\bar{\phi}$ will be approximated below via

$$\bar{\phi}_{\text{HS}} \approx \frac{4\rho^2 \theta}{\rho_{\text{HS}}}, \quad (81)$$

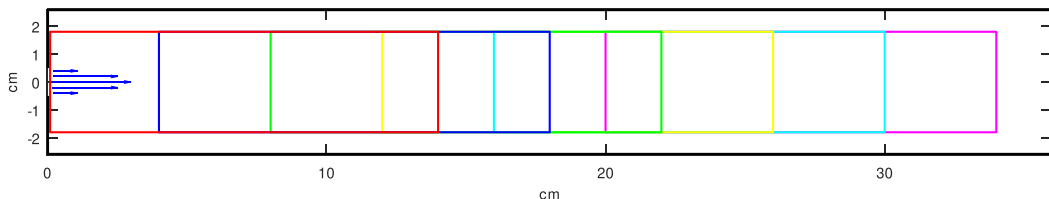


FIG. 1. The longitudinal section ($z = 0$) of the simulation domain. The domain dimensions are $36 \times 5.2 \times 5.2$ cm. The inlet is on the left, and the outlet is on the right. The pipe walls are shown via thick black lines, so that both the inlet and outlet are visible. The boundaries of the Fourier spectrum measurement regions are shown in different colors. Each region is a box of 14 cm in length, and 3.6×3.6 cm in cross section. The longitudinal offsets of regions are 0 (red), 4 (blue), 8 (green), 12 (yellow), 16 (cyan), and 20 (magenta) cm from the inlet.

which is the same formula as we used previously in [24,25]. For the hard-sphere mean field potential given via (81), the equations in (76) become

$$\frac{\partial \rho}{\partial t} + \nabla \cdot (\rho \mathbf{u}) = 0, \quad \frac{\partial (\theta^{-1})}{\partial t} + \nabla \cdot (\theta^{-1} \mathbf{u}) = 0, \quad (82a)$$

$$\frac{\partial (\rho \mathbf{u})}{\partial t} + \nabla \cdot (\rho \mathbf{u}^2) + \nabla \left[\rho \theta \left(1 + \frac{4\rho}{\rho_{\text{HS}}} \right) \right] = \mathbf{0}. \quad (82b)$$

The corresponding inertial flow equations in (77) become

$$\frac{\partial \rho}{\partial t} + \nabla \cdot (\rho \mathbf{u}) = 0, \quad \frac{\partial (\rho \mathbf{u})}{\partial t} + \nabla \cdot (\rho \mathbf{u}^2) + \frac{4p_0}{\rho_{\text{HS}}} \nabla \rho = \mathbf{0}. \quad (83)$$

Remarkably, one can verify that the potential forcing above in (83) acts in the direction of the temperature gradient, by substituting $\rho = p_0/\theta$ under the gradient of the potential term in (83). Thus, the forcing due to the intermolecular potential likely creates the thermal creep flow at constant pressure [52], and is possibly also responsible for the Soret effect [53]. We will, however, abstain from focusing on these interesting phenomena here since the goal of this work is to address the creation of turbulence instead.

VI. NUMERICAL SIMULATIONS OF THE INERTIAL FLOW IN A STRAIGHT PIPE

Here, we use the inertial flow equations with the hard-sphere mean field potential in (83) to simulate the flow of air in a straight pipe, with the parameters similar to those in the experiment by Buchhave and Velte [54]. We use the same computational software as in our previous works [24,25], namely, OPENFOAM[55]. Noting that the inertial flow equations in (83) comprise a system of nonlinear conservation laws, we simulate them with the help of the appropriately modified rhoCentralFoam solver [56], which uses the central scheme of Kurganov and Tadmor [57] for the numerical finite-volume discretization, with the flux limiter due to van Leer [58]. The time stepping of the method is adaptive, based on the 20% of the maximal Courant number.

A. Details of the computational implementation

We simulate the inertial flow equations with the hard-sphere mean field potential (83) in a straight pipe of a square cross section, with dimensions of $36 \times 5.2 \times 5.2$ cm. In the corresponding Cartesian reference frame, the x coordinate varies between 0 and 36 cm, while both the y and z coordinates vary between -2.6 and 2.6 cm. The longitudinal section of the domain (that is, what lies in the xy plane with $z = 0$) is shown in Fig. 1. The spatial discretization step is 0.8 mm in all three dimensions, totaling $450 \times 65 \times 65 = 1\,901\,250$ finite-volume cells.

The air enters the pipe through the round inlet of 1 cm in diameter, located in the middle of the square wall which lies in the yz plane (that is $x = 0$ cm). The air exits the pipe through a square 3.6×3.6 cm outlet, located in the middle of the opposite square wall at $x = 36$ cm (so that, within the outlet, both the y and z coordinates vary between -1.8 and 1.8 cm). Both the inlet and outlet are visible in Fig. 1 as gaps on the left- and right-hand sides of the plot. The length of the domain, together with the size and shape of the inlet, are consistent with those in the experiment of Buchhave and Velte [54].

In what follows, we compute the Fourier spectra of the streamwise kinetic energy and temperature in the six regions, distributed uniformly along the pipe. Each region is a box of 14 cm in length and 3.6×3.6 cm in cross section. The regions are situated on the longitudinal axis of the pipe with varying distances from the inlet wall: 0, 4, 8, 12, 16, and 20 cm. These regions are also displayed in Fig. 1 in different colors.

The constant parameters p_0 and ρ_{HS} in (83) are set, respectively, to 10^5 Pa (normal pressure), and 1850 kg/m^3 , based on the molar mass and viscosity of air (for details, see Abramov [25]). The following boundary conditions are used throughout the computation:

(i) *Inlet and walls.* For the density, we set the Neumann boundary condition with zero normal derivative. For the velocity, we set the Dirichlet boundary condition, with zero value at the walls, and a radially symmetric parabolic profile at the inlet, with the maximum value of 30 m/s at the center (as in the experiment of Buchhave and Velte [54]), directed along the x axis of the pipe.

(ii) *Outlet.* For the density, we set the Dirichlet boundary condition with the value of 1.209 kg/m^3 , which corresponds to the density of air at normal conditions (that is, the pressure 10^5 Pa and temperature 288.15 K, or 15 °C). For the velocity, we set the Neumann boundary condition with zero normal derivative.

At the start of the numerical simulation, the air inside the domain is at rest (zero velocity, 1.209 kg/m^3 density). This initial condition simulates a realistic laboratory scenario, where a jet enters the otherwise resting air. This is markedly different from what we used previously in [24,25], where the initial condition was a laminar jet inside the domain.

The reason why the outlet in our domain does not comprise the whole square wall, but rather forms a “window” in it, is the following. Given that the mathematical properties of (83) have not been studied in detail as of yet, the consistency of its boundary conditions is currently an open question. However, empirically, we found that, when the adjacent domain patches with different types of boundary conditions were transversal, a numerical instability developed in the vicinity of the adjoining edge. Conversely, we also found that, when such adjacent patches were located in the same plane, such numerical instability did not manifest. Thus, we implemented the window-type outlet at the end of the pipe to avoid the aforementioned numerical instability.

B. Results of the numerical simulation

As a benchmark, we first simulated the inertial flow equations in (83) without the mean field potential. In such a case, the velocity becomes decoupled from the density, and is governed by the standalone equation

$$\frac{\partial \mathbf{u}}{\partial t} + (\mathbf{u} \cdot \nabla) \mathbf{u} = \mathbf{0}. \quad (84)$$

The above equation does not, however, have the form of a conservation law, and thus the numerical simulation is still completed using (83) with the initial and boundary conditions set as described above in Sec. VI A, except that the mean field potential forcing is set to zero. In the same fashion as we did in [24], here we show the snapshots of the speed of the flow, captured in the xy plane of the pipe (that is, for $z = 0$), in the form of contour plots. The snapshots are taken at the times $t = 0.01, 0.02, 0.03,$ and 0.05 s of the elapsed time, and are shown in Fig. 2. As we can see, in the absence of the potential forcing, the jet “pierces” the resting air and exits through the outlet, remaining laminar in the process. Once the jet fully traverses the length of the pipe, the numerical solution reaches a

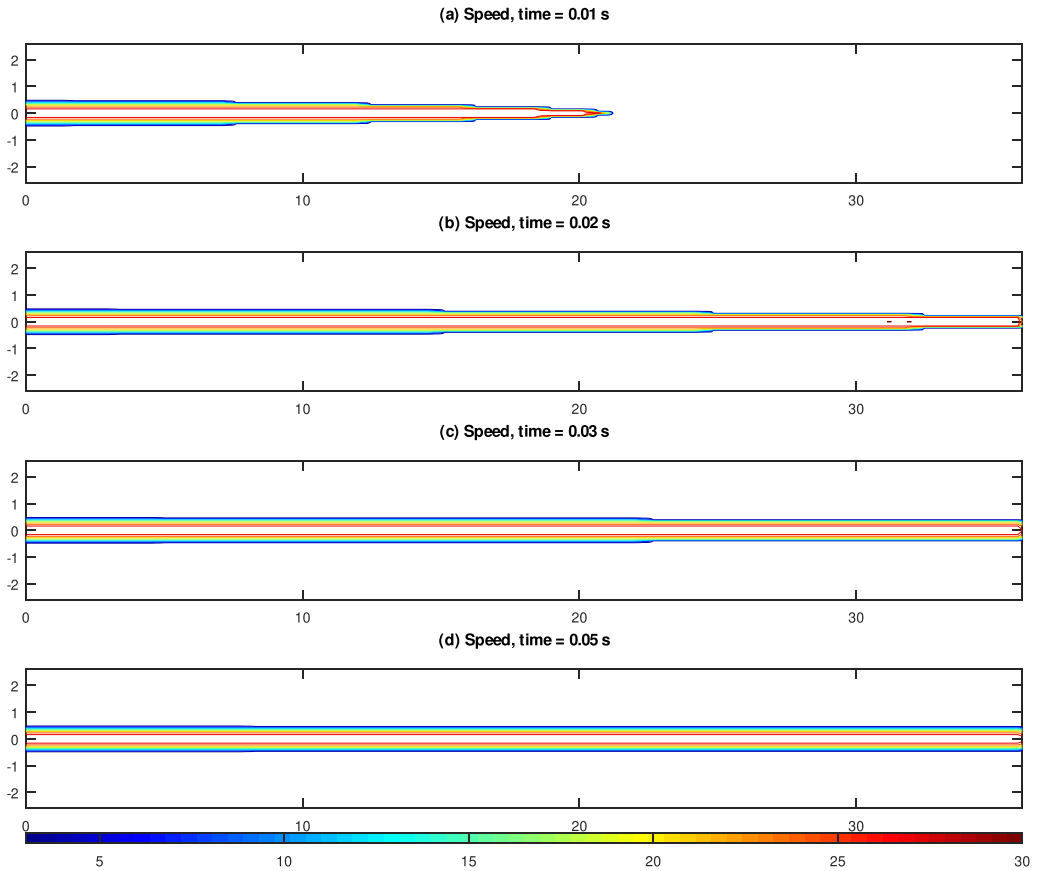


FIG. 2. Speed of the flow (m/s) without the mean field potential, captured in the xy plane ($z = 0$) of the pipe at (a) 0.01, (b) 0.02, (c) 0.03, and (d) 0.05 s of elapsed model time.

steady state. The air outside of the jet (that is, at the distance more than 0.5 cm from the axis of the pipe) remains at rest at all times.

For comparison, in Fig. 3, we show the speed of the flow in the same form as in Fig. 2, except that the potential forcing is set as described in Sec. VIA, with $p_0 = 10^5$ Pa and $\rho_{HS} = 1850$ kg/m³. As we can see, there is a remarkable difference between the plots. Once the potential forcing is present, the jet creates fluctuations around itself, disintegrating in the process, just as typically observed in nature and experiments [2,54], as well as in numerical simulations of our recent works [24,25]. The length of the pipe is such that the jet completely falls apart by the time the flow reaches the outlet; in fact, at time $t = 0.03$ s, the jet extends somewhat farther than in the subsequent snapshot, taken at time $t = 0.05$ s. By the time $t = 0.05$ s, the structure of the flow is as follows. In the first third of the pipe, the jet is largely intact, with small fluctuations around it. In the second third of the pipe, the jet disintegrates, transitioning into a chaotic flow. In the last third of the pipe, the flow is completely chaotic, with weak remnants of the jet, which can be observed in the middle of the pipe. After the time $t = 0.05$ s, the overall structure of the flow remained the same as the computation proceeded, and thus we concluded that the statistical steady state has been reached at $t = 0.05$. However, unlike the simulation without the potential shown in Fig. 2, here the flow never settles on a steady state, and remains in chaotic motion at all times.

The remarkable difference between the flows in Figs. 2 and 3 confirms that, at normal conditions, the effect of an intermolecular potential, expressed via the mean field forcing, is non-negligible and

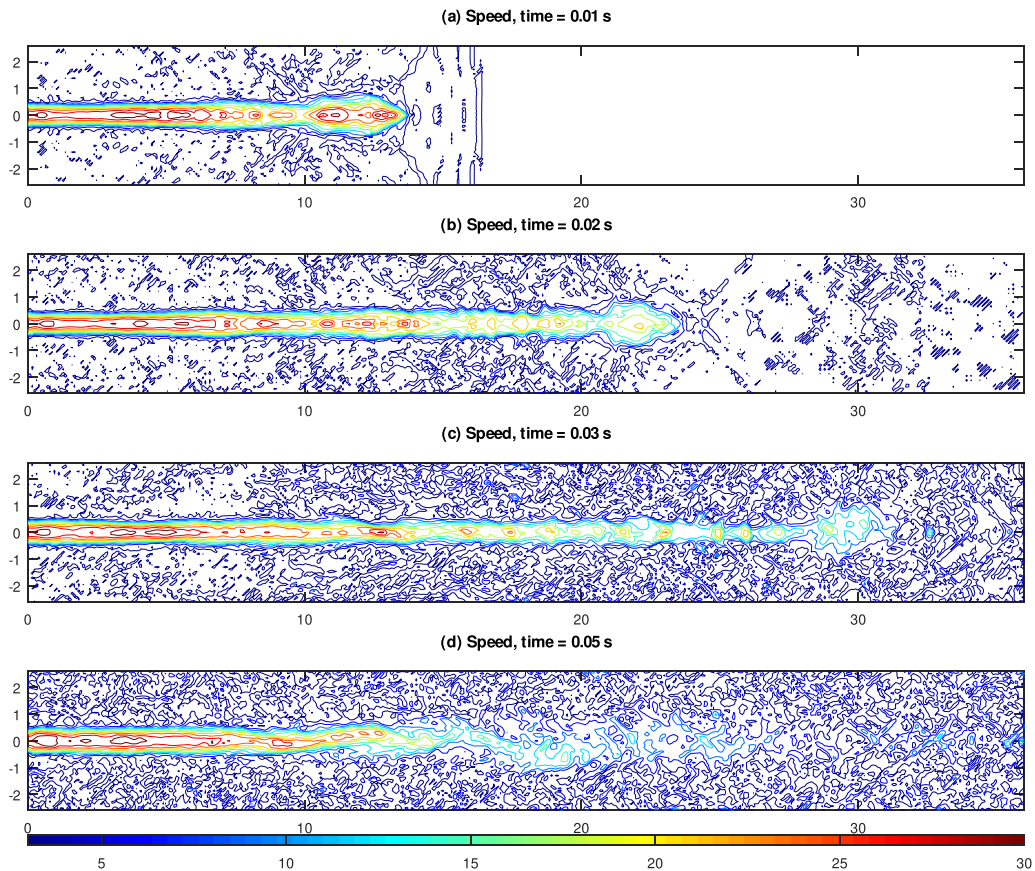


FIG. 3. Speed of the flow (m/s), captured in the xy plane ($z = 0$) of the pipe at (a) 0.01, (b) 0.02, (c) 0.03, and (d) 0.05 s of elapsed model time.

quantifiable. Furthermore, the presence of the mean field potential unambiguously creates turbulent motions in the numerical simulation of an inertial flow, and these motions are similar to those observed in nature and experiments.

In addition, observe that the geometry of the domain, as well as the initial and boundary conditions, are symmetric with respect to the central axis of the pipe. This means that, technically, the flow must also remain symmetric relative to the central axis at all times. However, it remains symmetric only in the absence of the intermolecular potential (see Fig. 2). When the intermolecular potential is present, we observe that the flow symmetry breaks as early as at $t = 0.02$ s [Fig. 3(b), small fluctuations near the outlet]. This breaking of the symmetry is a reliable indication of a strongly chaotic dynamics: what we observe is roundoff errors of the floating point arithmetic, which introduce a very weak asymmetry into the numerical solution, grow exponentially rapidly in time due to large positive Lyapunov exponents. As an example, a similar phenomenon manifested in the work of Majda and Timofeyev [59], where the initial condition from a low-dimensional stable manifold of the truncated Burgers-Hopf system evolved into a fully chaotic and mixing solution due to the exponential growth of machine roundoff errors (for a more detailed explanation, see [60], Sec. 2.2.4).

1. Density of the flow

In addition to the snapshots of the flow speed, in Fig. 4 we show the snapshots of the density of the flow, captured in the same way and at the same times, and also displayed as contour plots.

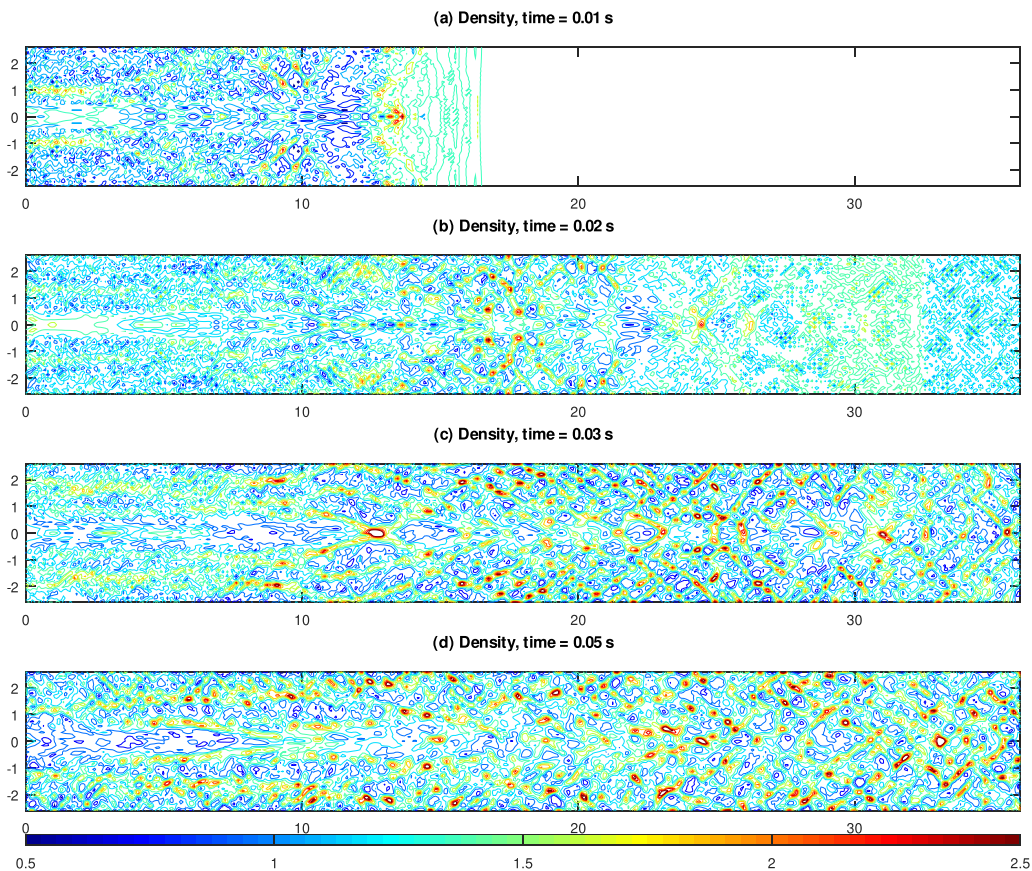


FIG. 4. Density of the flow (kg/m^3), captured in the xy plane ($z = 0$) of the pipe at (a) 0.01, (b) 0.02, (c) 0.03, and (d) 0.05 s of elapsed model time.

Just as in our recent works [24,25], observe that the fluctuations of density from its background value of $1.209 \text{ kg}/\text{m}^3$ are rather unrealistic, as much as by a factor of 2 both ways. We currently presume that this happens due to that fact that our model is “too idealized”; namely, the pressure is presumed to be strictly constant irrespectively of how the other variables behave. In a real gas, obviously, such condition may not strictly hold: if a large enough density gradient develops locally in a flow, it would also inevitably create a pressure fluctuation. Our simplified model, on the other hand, adheres strictly to Charles’ law for a constant pressure process, and thus has certain bounds of practical applicability. Generally, it appears to be a challenging problem to create a universal gas transport model, which would be accurate in all thermodynamic regimes of the flow, from Charles’ law at low Mach numbers, to acoustic waves and adiabatic shock transitions at high Mach numbers.

2. Fourier spectra of the kinetic energy

Here, we show the time averages of the Fourier spectra of the streamwise kinetic energy of the flow (that is, the energy of the x component of the velocity), computed in the six regions which were described in Sec. VIA and shown in Fig. 1. In each region, the kinetic energy spectrum was computed as follows: first, the kinetic energy of the x component of the velocity $E_x = u_x^2/2$, was averaged over the cross section of the region, thus becoming the function of the x coordinate only. Then, the linear trend was subtracted from the result in the same manner as was done by Nastrom and Gage [61] and also in our recent works [24,25], to ensure that there was no sharp

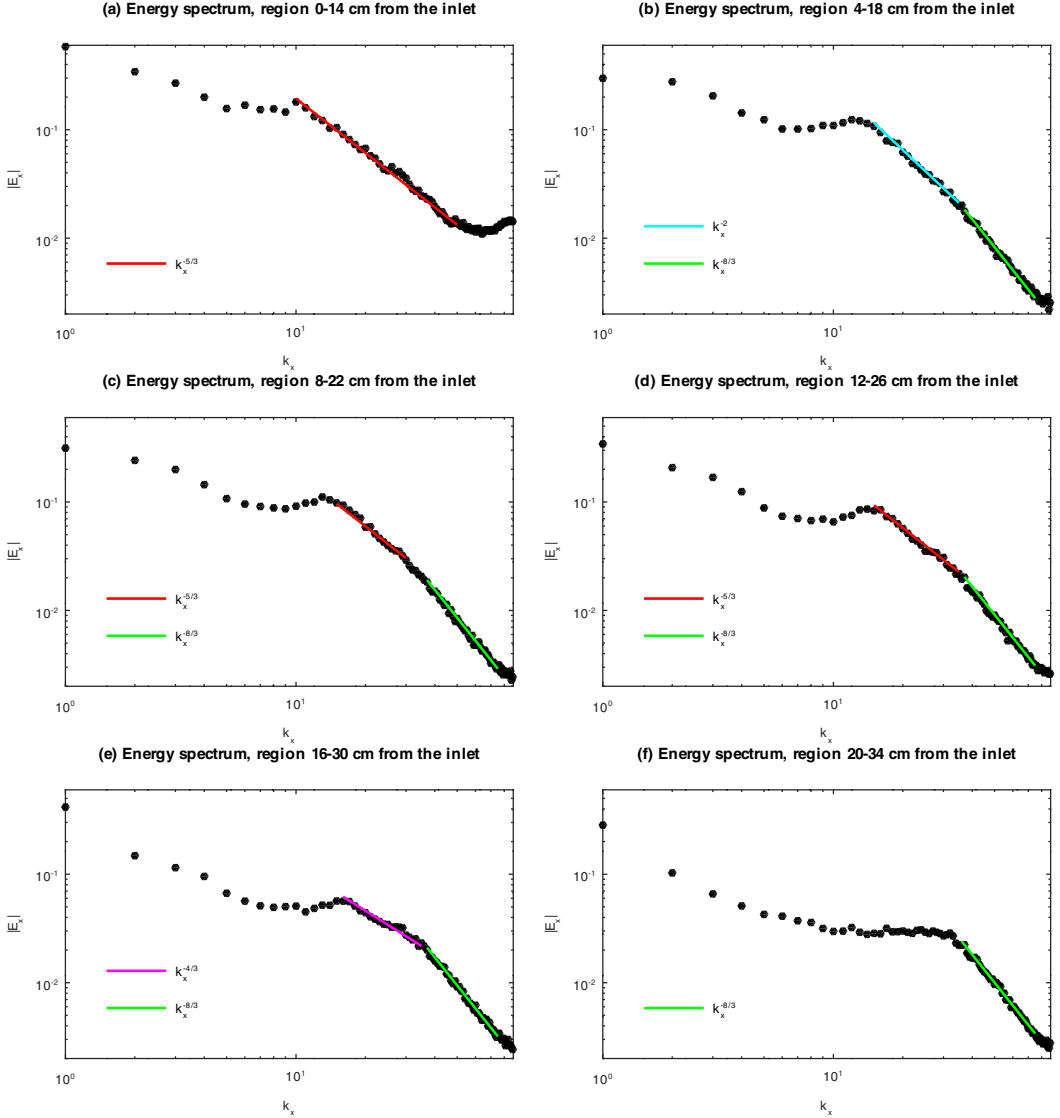


FIG. 5. The Fourier spectra of the kinetic energy, computed within different spatial windows, situated at (a) 0–14, (b) 4–18, (c) 8–22, (d) 12–26, (e) 16–30, and (f) 20–34 cm, counting from the inlet. The slope lines $k^{-5/3}$, k^{-2} , $k^{-4/3}$, and $k^{-8/3}$ are given for the reference.

discontinuity between the energy values at the western and eastern boundaries of the region. Finally, the one-dimensional discrete Fourier transformation was applied to the result. The subsequent time averaging of the modulus of the Fourier transform was computed in the time interval $0.1 \leq t \leq 0.2$ s of the elapsed model time.

The time averages of the kinetic energy spectra, computed as described above, are shown in Fig. 5 for all six regions, in the ascending order of their distance from the inlet. In the first region, which begins directly at the inlet [Fig. 5(a)], the kinetic energy spectrum has the decay of $k_x^{-5/3}$ (the famous Kolmogorov spectrum) on the moderate and small scales, and looks very similar to what was observed by Buchhave and Velte [54] in their experiment, and simulated in our recent work [24] for the flow of argon. However, as the measurement region shifts away from the inlet, a qualitative

change in the kinetic energy spectra is observed: the decay rates become different between the moderate and small scales. At the small scales, starting approximately with the wave number 35 and up, the decay rate of the kinetic energy corresponds to $k_x^{-8/3}$ in all remaining measurement regions, and looks similar to what we observed in our recent work [25] for a large-scale two-dimensional flow. However, at the moderate scales (between the wave numbers 15 and 35, approximately) the power of the decay rate varies between different regions:

- (1) In the region beginning at 4 cm from the outlet [Fig. 5(b)], the rate of decay corresponds to k_x^{-2} .
- (2) In the regions beginning at 8 and 12 cm from the outlet [Figs. 5(c) and 5(d)], the rate of decay corresponds to $k_x^{-5/3}$.
- (3) In the region beginning at 16 cm from the outlet [Fig. 5(e)], the rate of decay becomes k_x^{-1} .
- (4) In the region beginning at 20 cm from the outlet [Fig. 5(f)], there is no decay at the moderate scales; the spectrum is flat.

Such two-tiered kinetic energy spectra, with steeper decay at small scales, were observed in the Jovian atmosphere by Cassini [62] and Juno [63] missions.

3. Fourier spectra of the temperature

In addition to the kinetic energy spectra of the large-scale meridional and zonal winds, Nastrom and Gage [61] reported the Fourier spectra of the temperature, and found that the latter also had power scaling. Therefore, in this work, we also report the time-averaged Fourier spectra of the temperature, which are computed in the precisely same manner as those of the kinetic energy, presented above. The temperature T (in K) is computed via the formula

$$T = \frac{M p_0}{R \rho}, \quad (85)$$

where $R = 8.31446 \text{ kg m}^2/\text{s}^2 \text{ mol K}$ is the universal gas constant, and $M = 2.897 \text{ kg/mol}$ is the molar mass of air.

We show the temperature spectra in Fig. 6, computed in the same measurement regions as shown in Fig. 1. As we can see, in the first measurement region, which extends from 0 to 14 cm, counting from the inlet, the rate of decay of the temperature spectrum largely corresponds to $k_x^{-5/3}$ [Fig. 6(a)]. However, a “two-tiered” decay is observed in the rest of the measurement regions, where, contrary to what was observed above for the kinetic energy, the steeper decay of k_x^{-2} and $k_x^{-8/3}$ is observed at the moderate scales (between the wave numbers 25 and 45, approximately). At small scales, the temperature spectrum decay corresponds to $k_x^{-5/3}$ for all measurement regions. We note that this power structure of the temperature spectrum (with slower decay rate at smaller scales) is similar to what was observed by Nastrom and Gage [61].

VII. SUMMARY

In this work, we extend our previous results in [24,25] onto polyatomic gas flows. We develop a tractable kinetic model of a general polyatomic gas, which describes the translational interaction via a deterministic intermolecular potential, and rotational interactions via stochastic collisions. In the suitable hydrodynamic limit for the distribution function of a single particle, we arrive at what we refer to as the Boltzmann-Vlasov equation, because our kinetic equation possesses both the deterministic potential and the stochastic collision integral. For the transport equations of velocity moments, we introduce a heat-flux closure by prescribing the appropriate specific-heat capacity of the process. For the specific-heat capacity taken at a constant pressure, we obtain the inertial flow equations of the same form as in [24], albeit with a slightly more accurate estimate of the mean field potential, which now includes the cavity distribution function.

For the numerical simulation, we choose a scenario which roughly corresponds to the experiment of Buchhave and Velte [54]. The air at normal conditions enters a straight pipe through the inlet of

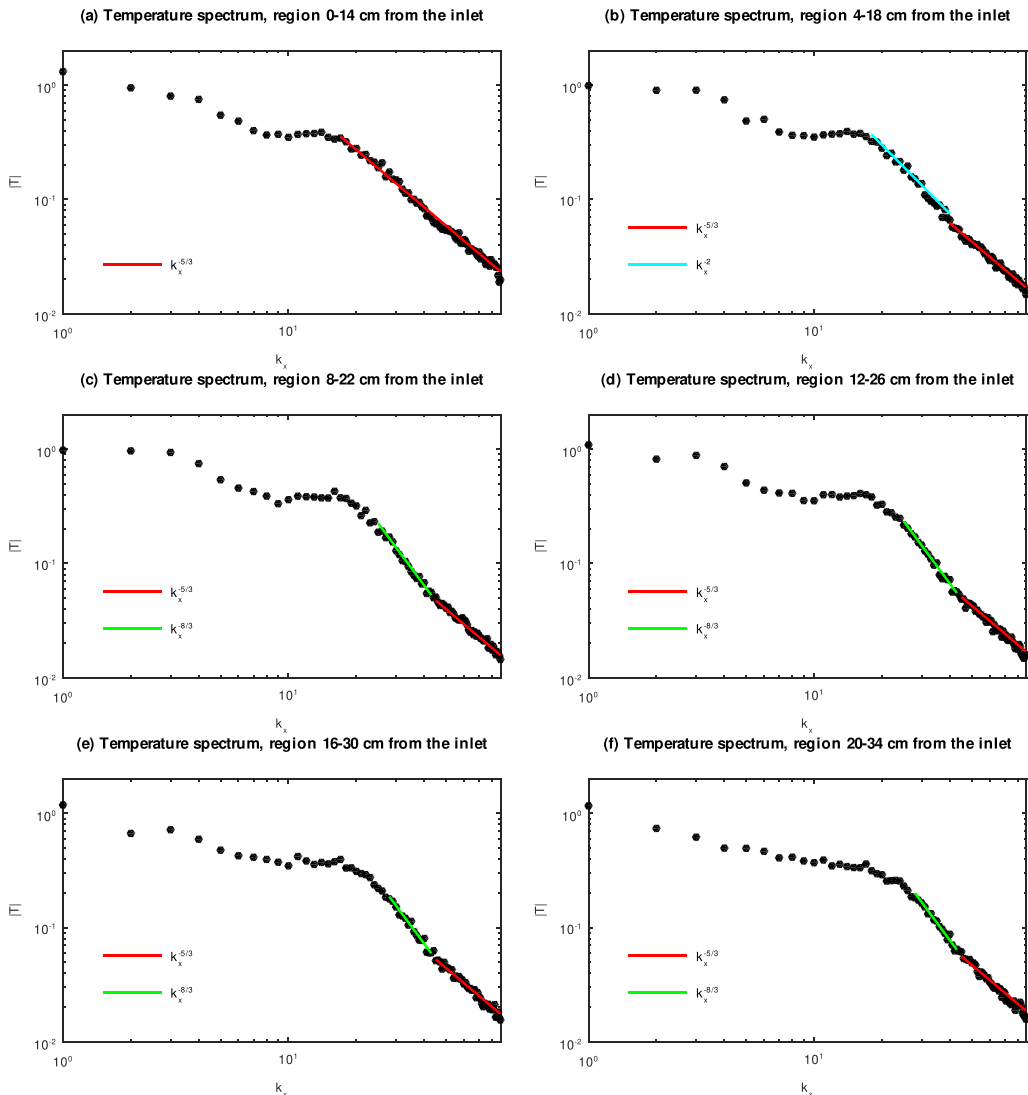


FIG. 6. The Fourier spectra of the temperature, computed within different spatial windows, situated at (a) 0–14, (b) 4–18, (c) 8–22, (d) 12–26, (e) 16–30, and (f) 20–34 cm, counting from the inlet. The slope lines $k^{-5/3}$, k^{-2} , and $k^{-8/3}$ are given for reference.

1 cm in diameter, with the parabolic velocity profile at the maximum speed of 30 m/s. We show that, in the absence of an interaction potential, the resulting laminar jet “pierces” the resting air and exits through the outlet; yet, in the presence of the interaction potential, the jet quickly breaks up into turbulent motions similarly to the results in our recent works [24,25]. We record the kinetic energy spectra within measurement regions at different distances from the inlet, and find a variety of different power spectra (in particular, a double-slope decay similar to that observed on Jupiter [62,63]). We also measure the temperature spectra of the flow in the same fashion, and observe that the structure of the power decay is similar to that observed in the Earth atmosphere [61].

ACKNOWLEDGMENT

This work was supported by the Simons Foundation Grant No. 636144.

APPENDIX A: ENTROPY INEQUALITY FOR THE FORWARD KOLMOGOROV EQUATION

To obtain the entropy inequalities in (22) for the forward Kolmogorov equation (18), let us consider the quantity

$$Q[\Psi_1(F), \Psi_2(F_0)] = \int \Psi_1(F)\Psi_2(F_0)d\mathbf{X} d\mathbf{V}, \quad (\text{A1})$$

where F_0 is a steady state of (18), and $\Psi_1 : \mathbb{R} \rightarrow \mathbb{R}$ and $\Psi_2 : \mathbb{R} \rightarrow \mathbb{R}$ are two differentiable functions. The time derivative of Q is given via

$$\begin{aligned} \frac{\partial}{\partial t} Q[\Psi_1(F), \Psi_2(F_0)] &= \int D\Psi_1(F) \frac{\partial F}{\partial t} \Psi_2(F_0) d\mathbf{X} d\mathbf{V} = \int D\Psi_1(F) \Psi_2(F_0) \\ &\times \left(\frac{\partial \Phi}{\partial \mathbf{X}} \cdot \frac{\partial F}{\partial \mathbf{V}} - \mathbf{V} \cdot \frac{\partial F}{\partial \mathbf{X}} + \sum_{i=1}^{K-1} \sum_{j=i+1}^K \lambda_{ij} [F(C_{ij}^{-1}\mathbf{V}) - F(\mathbf{V})] \right) d\mathbf{X} d\mathbf{V}, \end{aligned} \quad (\text{A2})$$

where the notation $D\Psi_1$ denotes the derivative of Ψ_1 with respect to its argument. Observe that the part of the latter integral which does not involve collisions is zero; indeed, the integration by parts yields

$$\begin{aligned} &\int D\Psi_1(F) \Psi_2(F_0) \left(\frac{\partial \Phi}{\partial \mathbf{X}} \cdot \frac{\partial F}{\partial \mathbf{V}} - \mathbf{V} \cdot \frac{\partial F}{\partial \mathbf{X}} \right) d\mathbf{X} d\mathbf{V} \\ &= \int \Psi_1(F) D\Psi_2(F_0) \left(\mathbf{V} \cdot \frac{\partial F_0}{\partial \mathbf{X}} - \frac{\partial \Phi}{\partial \mathbf{X}} \cdot \frac{\partial F_0}{\partial \mathbf{V}} \right) d\mathbf{X} d\mathbf{V} = 0. \end{aligned} \quad (\text{A3})$$

For the collision term, we use the fact that both λ_{ij} and F_0 are invariant under C_{ij} , and obtain

$$\frac{\partial}{\partial t} Q[\Psi_1(F), \Psi_2(F_0)] = \sum_{i=1}^{K-1} \sum_{j=i+1}^K \int \lambda_{ij} F [D\Psi_1(F(C_{ij}(\mathbf{V}))) - D\Psi_1(F(\mathbf{V}))] \Psi_2(F_0) d\mathbf{X} d\mathbf{V}. \quad (\text{A4})$$

Clearly, for some special cases of Ψ_1 and Ψ_2 , the expression above can be treated further. The most obvious simplification occurs when $\Psi_1(F) = F$, in which case the expression above is zero irrespective of Ψ_2 :

$$\frac{\partial}{\partial t} Q[F, \Psi_2(F_0)] = 0. \quad (\text{A5})$$

Next, let us consider the special case with $\Psi_1(F) = -F \ln F$, $\Psi_2(F_0) = 1$, such that Q is the Shannon entropy. In this case, we prove the first statement in (22):

$$\begin{aligned} -\frac{\partial}{\partial t} \int F \ln F d\mathbf{X} d\mathbf{V} &= \sum_{i=1}^{K-1} \sum_{j=i+1}^K \int \lambda_{ij} F(\mathbf{V}) \ln \left(\frac{F(\mathbf{V})}{F(C_{ij}(\mathbf{V}))} \right) d\mathbf{X} d\mathbf{V} \\ &\geq \sum_{i=1}^{K-1} \sum_{j=i+1}^K \int \lambda_{ij} F(C_{ij}(\mathbf{V})) \left(\frac{F(\mathbf{V})}{F(C_{ij}(\mathbf{V}))} - 1 \right) d\mathbf{X} d\mathbf{V} = 0, \end{aligned} \quad (\text{A6})$$

where we used the inequality $x \ln x \geq x - 1$. Setting $\Psi_2(F_0) = \ln F_0$ in (A5), and subtracting (A6), yields the second statement in (22).

APPENDIX B: HYDRODYNAMIC LIMIT FOR THE BOLTZMANN-VLASOV EQUATION

Here we compute the integral in the right-hand side of (35), with the rescalings in (36).

1. Potential forcing

Upon replacing the dummy variable of integration $\mathbf{x}_2 = \mathbf{x} - \sigma \mathbf{r}$, the integral for the potential forcing in the right-hand side of (35) becomes

$$\begin{aligned} & \frac{1}{m} \int e^{-\frac{\phi(\|\mathbf{x}-\mathbf{x}_2\|/\sigma)}{\theta(\|\mathbf{x}+\mathbf{x}_2\|/2)}} Y_K(\theta(\|\mathbf{x}+\mathbf{x}_2\|/2), \|\mathbf{x}-\mathbf{x}_2\|/\sigma) \frac{\partial}{\partial \mathbf{x}} \phi(\|\mathbf{x}-\mathbf{x}_2\|/\sigma) \rho(\mathbf{x}_2) d\mathbf{x}_2 \\ &= \frac{\sigma^2}{m} \int e^{-\frac{\phi(\|\mathbf{r}\|)}{\theta(\mathbf{x}-\sigma\mathbf{r}/2)}} Y_K(\theta(\mathbf{x}-\sigma\mathbf{r}/2), \|\mathbf{r}\|) \frac{\partial \phi(\|\mathbf{r}\|)}{\partial \mathbf{r}} \rho(\mathbf{x}-\sigma\mathbf{r}) d\mathbf{r}. \end{aligned} \quad (\text{B1})$$

Next, we observe that

$$\begin{aligned} e^{-\frac{\phi(\|\mathbf{r}\|)}{\theta(\mathbf{x}-\sigma\mathbf{r}/2)}} \frac{\partial \phi(\|\mathbf{r}\|)}{\partial \mathbf{r}} &= e^{-\frac{\phi(\|\mathbf{r}\|)}{\theta(\mathbf{x}-\sigma\mathbf{r}/2)}} \theta(\mathbf{x}-\sigma\mathbf{r}/2) \left(\frac{\sigma}{2} \frac{\partial}{\partial \mathbf{x}} + \frac{\partial}{\partial \mathbf{r}} \right) \left(\frac{\phi(\|\mathbf{r}\|)}{\theta(\mathbf{x}-\sigma\mathbf{r}/2)} \right) \\ &= \theta(\mathbf{x}-\sigma\mathbf{r}/2) \left(\frac{\sigma}{2} \frac{\partial}{\partial \mathbf{x}} + \frac{\partial}{\partial \mathbf{r}} \right) (1 - e^{-\frac{\phi(\|\mathbf{r}\|)}{\theta(\mathbf{x}-\sigma\mathbf{r}/2)}}). \end{aligned} \quad (\text{B2})$$

We now can now manipulate the integral as follows:

$$\begin{aligned} & \frac{\sigma^2}{m} \int e^{-\frac{\phi(\|\mathbf{r}\|)}{\theta(\mathbf{x}-\sigma\mathbf{r}/2)}} Y_K(\theta(\mathbf{x}-\sigma\mathbf{r}/2), \|\mathbf{r}\|) \frac{\partial \phi(\|\mathbf{r}\|)}{\partial \mathbf{r}} \rho(\mathbf{x}-\sigma\mathbf{r}) d\mathbf{r} \\ &= \frac{\sigma^3}{2m} \int Y_K(\theta(\mathbf{x}-\sigma\mathbf{r}/2), \|\mathbf{r}\|) \theta(\mathbf{x}-\sigma\mathbf{r}/2) \rho(\mathbf{x}-\sigma\mathbf{r}) \frac{\partial}{\partial \mathbf{x}} (1 - e^{-\frac{\phi(\|\mathbf{r}\|)}{\theta(\mathbf{x}-\sigma\mathbf{r}/2)}}) d\mathbf{r} \\ &+ \frac{\sigma^2}{m} \int Y_K(\theta(\mathbf{x}-\sigma\mathbf{r}/2), \|\mathbf{r}\|) \theta(\mathbf{x}-\sigma\mathbf{r}/2) \rho(\mathbf{x}-\sigma\mathbf{r}) \frac{\partial}{\partial \mathbf{r}} (1 - e^{-\frac{\phi(\|\mathbf{r}\|)}{\theta(\mathbf{x}-\sigma\mathbf{r}/2)}}) d\mathbf{r}. \end{aligned} \quad (\text{B3})$$

The first integral above can be expressed via

$$\begin{aligned} & \frac{\sigma^3}{2m} \int Y_K(\theta(\mathbf{x}-\sigma\mathbf{r}/2), \|\mathbf{r}\|) \theta(\mathbf{x}-\sigma\mathbf{r}/2) \rho(\mathbf{x}-\sigma\mathbf{r}) \frac{\partial}{\partial \mathbf{x}} (1 - e^{-\frac{\phi(\|\mathbf{r}\|)}{\theta(\mathbf{x}-\sigma\mathbf{r}/2)}}) d\mathbf{r} \\ &= \frac{\sigma^3}{2m} \frac{\partial}{\partial \mathbf{x}} \int Y_K(\theta(\mathbf{x}-\sigma\mathbf{r}/2), \|\mathbf{r}\|) \theta(\mathbf{x}-\sigma\mathbf{r}/2) \rho(\mathbf{x}-\sigma\mathbf{r}) (1 - e^{-\frac{\phi(\|\mathbf{r}\|)}{\theta(\mathbf{x}-\sigma\mathbf{r}/2)}}) d\mathbf{r} \\ &- \frac{\sigma^3}{2m} \int (1 - e^{-\frac{\phi(\|\mathbf{r}\|)}{\theta(\mathbf{x}-\sigma\mathbf{r}/2)}}) \frac{\partial}{\partial \mathbf{x}} [Y_K(\theta(\mathbf{x}-\sigma\mathbf{r}/2), \|\mathbf{r}\|) \theta(\mathbf{x}-\sigma\mathbf{r}/2) \rho(\mathbf{x}-\sigma\mathbf{r})] d\mathbf{r} \\ &= \frac{\sigma^3}{2m} \frac{\partial}{\partial \mathbf{x}} \int Y_K(\theta(\mathbf{x}-\sigma\mathbf{r}/2), \|\mathbf{r}\|) \theta(\mathbf{x}-\sigma\mathbf{r}/2) \rho(\mathbf{x}-\sigma\mathbf{r}) (1 - e^{-\frac{\phi(\|\mathbf{r}\|)}{\theta(\mathbf{x}-\sigma\mathbf{r}/2)}}) d\mathbf{r} \\ &+ \frac{\sigma^2}{m} \int (1 - e^{-\frac{\phi(\|\mathbf{r}\|)}{\theta(\mathbf{x}-\sigma\mathbf{r}/2)}}) \left(-\frac{\sigma}{2} \right) \frac{\partial}{\partial \mathbf{x}} [Y_K(\theta(\mathbf{x}-\sigma\mathbf{r}/2), \|\mathbf{r}\|) \theta(\mathbf{x}-\sigma\mathbf{r}/2) \rho(\mathbf{x}-\sigma\mathbf{r})] d\mathbf{r}, \end{aligned} \quad (\text{B4})$$

where we observe that

$$\begin{aligned} & -\frac{\sigma}{2} \frac{\partial}{\partial \mathbf{x}} [Y_K(\theta(\mathbf{x}-\sigma\mathbf{r}/2), \|\mathbf{r}\|) \theta(\mathbf{x}-\sigma\mathbf{r}/2) \rho(\mathbf{x}-\sigma\mathbf{r})] \\ &= \frac{\partial}{\partial \mathbf{r}} [Y_K(\theta(\mathbf{x}-\sigma\mathbf{r}/2), \|\mathbf{r}\|) \theta(\mathbf{x}-\sigma\mathbf{r}/2) \rho(\mathbf{x}-\sigma\mathbf{r})] \\ &- \theta(\mathbf{x}-\sigma\mathbf{r}/2) \rho(\mathbf{x}-\sigma\mathbf{r}) \frac{\partial}{\partial \mathbf{r}} Y_K(\theta(\mathbf{x}-\sigma\mathbf{r}/2), \|\mathbf{r}\|) \frac{\mathbf{r}}{\|\mathbf{r}\|} \\ &+ \frac{\sigma}{2} Y_K(\theta(\mathbf{x}-\sigma\mathbf{r}/2), \|\mathbf{r}\|) \theta(\mathbf{x}-\sigma\mathbf{r}/2) \frac{\partial}{\partial \mathbf{x}} \rho(\mathbf{x}-\sigma\mathbf{r}). \end{aligned} \quad (\text{B5})$$

The second integral can be integrated by parts:

$$\begin{aligned} & \frac{\sigma^2}{m} \int Y_K(\theta(\mathbf{x} - \sigma \mathbf{r}/2), \|\mathbf{r}\|) \theta(\mathbf{x} - \sigma \mathbf{r}/2) \rho(\mathbf{x} - \sigma \mathbf{r}) \frac{\partial}{\partial \mathbf{r}} (1 - e^{-\frac{\phi(\|\mathbf{r}\|)}{\theta(\mathbf{x} - \sigma \mathbf{r}/2)}}) d\mathbf{r} \\ &= -\frac{\sigma^2}{m} \int (1 - e^{-\frac{\phi(\|\mathbf{r}\|)}{\theta(\mathbf{x} - \sigma \mathbf{r}/2)}}) \frac{\partial}{\partial \mathbf{r}} [Y_K(\theta(\mathbf{x} - \sigma \mathbf{r}/2), \|\mathbf{r}\|) \theta(\mathbf{x} - \sigma \mathbf{r}/2) \rho(\mathbf{x} - \sigma \mathbf{r})] d\mathbf{r}. \end{aligned} \quad (\text{B6})$$

Thus, (B1) is given via

$$\begin{aligned} & \frac{\sigma^2}{m} \int e^{-\frac{\phi(\|\mathbf{r}\|)}{\theta(\mathbf{x} - \sigma \mathbf{r}/2)}} Y_K(\theta(\mathbf{x} - \sigma \mathbf{r}/2), \|\mathbf{r}\|) \frac{\partial \phi(\|\mathbf{r}\|)}{\partial \mathbf{r}} \rho(\mathbf{x} - \sigma \mathbf{r}) d\mathbf{r} \\ &= \frac{\sigma^3}{2m} \frac{\partial}{\partial \mathbf{x}} \int Y_K(\theta(\mathbf{x} - \sigma \mathbf{r}/2), \|\mathbf{r}\|) \theta(\mathbf{x} - \sigma \mathbf{r}/2) \rho(\mathbf{x} - \sigma \mathbf{r}) (1 - e^{-\frac{\phi(\|\mathbf{r}\|)}{\theta(\mathbf{x} - \sigma \mathbf{r}/2)}}) d\mathbf{r} \\ &+ \frac{\sigma^3}{2m} \int Y_K(\theta(\mathbf{x} - \sigma \mathbf{r}/2), \|\mathbf{r}\|) \theta(\mathbf{x} - \sigma \mathbf{r}/2) (1 - e^{-\frac{\phi(\|\mathbf{r}\|)}{\theta(\mathbf{x} - \sigma \mathbf{r}/2)}}) \frac{\partial}{\partial \mathbf{x}} \rho(\mathbf{x} - \sigma \mathbf{r}) d\mathbf{r} \\ &- \frac{\sigma^2}{m} \int (1 - e^{-\frac{\phi(\|\mathbf{r}\|)}{\theta(\mathbf{x} - \sigma \mathbf{r}/2)}}) \theta(\mathbf{x} - \sigma \mathbf{r}/2) \rho(\mathbf{x} - \sigma \mathbf{r}) \frac{\partial}{\partial \mathbf{r}} Y_K(\theta(\mathbf{x} - \sigma \mathbf{r}/2), \|\mathbf{r}\|) \frac{\mathbf{r}}{\|\mathbf{r}\|} d\mathbf{r}. \end{aligned} \quad (\text{B7})$$

The sum of the first two integrals in the right-hand side above is

$$\begin{aligned} & \frac{\sigma^3}{2m} \frac{\partial}{\partial \mathbf{x}} \int Y_K(\theta(\mathbf{x} - \sigma \mathbf{r}/2), \|\mathbf{r}\|) \theta(\mathbf{x} - \sigma \mathbf{r}/2) \rho(\mathbf{x} - \sigma \mathbf{r}) (1 - e^{-\frac{\phi(\|\mathbf{r}\|)}{\theta(\mathbf{x} - \sigma \mathbf{r}/2)}}) d\mathbf{r} \\ &+ \frac{\sigma^3}{2m} \int Y_K(\theta(\mathbf{x} - \sigma \mathbf{r}/2), \|\mathbf{r}\|) \theta(\mathbf{x} - \sigma \mathbf{r}/2) (1 - e^{-\frac{\phi(\|\mathbf{r}\|)}{\theta(\mathbf{x} - \sigma \mathbf{r}/2)}}) \frac{\partial}{\partial \mathbf{x}} \rho(\mathbf{x} - \sigma \mathbf{r}) d\mathbf{r} \\ &= \frac{\sigma^3}{2m} \int \frac{1}{\rho(\mathbf{x} - \sigma \mathbf{r})} \frac{\partial}{\partial \mathbf{x}} [Y_K(\theta(\mathbf{x} - \sigma \mathbf{r}/2), \|\mathbf{r}\|) \theta(\mathbf{x} - \sigma \mathbf{r}/2) \rho^2(\mathbf{x} - \sigma \mathbf{r}) (1 - e^{-\frac{\phi(\|\mathbf{r}\|)}{\theta(\mathbf{x} - \sigma \mathbf{r}/2)}})] d\mathbf{r} \\ &\rightarrow 2\pi \frac{\sigma^3}{m} \frac{1}{\rho(\mathbf{x})} \frac{\partial}{\partial \mathbf{x}} \left[\theta(\mathbf{x}) \rho^2(\mathbf{x}) \int_0^\infty Y(\theta(\mathbf{x}), r) (1 - e^{-\frac{\phi(r)}{\theta(\mathbf{x})}}) r^2 dr \right], \end{aligned} \quad (\text{B8})$$

as $\sigma \rightarrow 0$ and $K \rightarrow \infty$, with σ^3/m being fixed. The second integral becomes, upon expanding in powers of σ and taking the same limit,

$$\begin{aligned} & -\frac{\sigma^2}{m} \int (1 - e^{-\frac{\phi(\|\mathbf{r}\|)}{\theta(\mathbf{x} - \sigma \mathbf{r}/2)}}) \theta(\mathbf{x} - \sigma \mathbf{r}/2) \rho(\mathbf{x} - \sigma \mathbf{r}) \frac{\partial}{\partial \mathbf{r}} Y_K(\theta(\mathbf{x} - \sigma \mathbf{r}/2), \|\mathbf{r}\|) \frac{\mathbf{r}}{\|\mathbf{r}\|} d\mathbf{r} \\ &= -\frac{\sigma^2}{m} \int (1 - e^{-\frac{\phi(\|\mathbf{r}\|)}{\theta(\mathbf{x})}}) \theta(\mathbf{x}) \rho(\mathbf{x}) \frac{\partial}{\partial \mathbf{r}} Y_K(\theta(\mathbf{x}), \|\mathbf{r}\|) \frac{\mathbf{r}}{\|\mathbf{r}\|} d\mathbf{r} \\ &+ \frac{\sigma^3}{2m} \frac{1}{\rho(\mathbf{x})} \frac{\partial}{\partial \mathbf{x}} \left[\theta(\mathbf{x}) \rho^2(\mathbf{x}) \int (1 - e^{-\frac{\phi(\|\mathbf{r}\|)}{\theta(\mathbf{x})}}) \frac{\partial}{\partial \mathbf{r}} Y_K(\theta(\mathbf{x}), \|\mathbf{r}\|) \cdot \frac{\mathbf{r}^2}{\|\mathbf{r}\|} d\mathbf{r} \right] + O(\sigma^4/m) \\ &\rightarrow \frac{\sigma^3}{2m} \frac{1}{\rho(\mathbf{x})} \frac{\partial}{\partial \mathbf{x}} \cdot \left[\theta(\mathbf{x}) \rho^2(\mathbf{x}) \int (1 - e^{-\frac{\phi(r)}{\theta(\mathbf{x})}}) \frac{\partial}{\partial r} Y(\theta(\mathbf{x}), r) r^3 dr \mathbf{n}^2 d\mathbf{n} \right], \end{aligned} \quad (\text{B9})$$

where \mathbf{n} is a unit vector, and the integration over $d\mathbf{n}$ occurs over a unit sphere. We recognize that

$$\int \mathbf{n}^2 d\mathbf{n} = \frac{4\pi}{3} \mathbf{I}, \quad (\text{B10})$$

and thus

$$\begin{aligned} & \frac{\sigma^3}{2m} \frac{1}{\rho(\mathbf{x})} \frac{\partial}{\partial \mathbf{x}} \cdot \left[\theta(\mathbf{x}) \rho^2(\mathbf{x}) \int (1 - e^{-\frac{\phi(r)}{\theta(\mathbf{x})}}) \frac{\partial}{\partial r} Y(\theta(\mathbf{x}), r) r^3 dr \mathbf{n}^2 d\mathbf{n} \right] \\ & = 2\pi \frac{\sigma^3}{m} \frac{\partial}{\partial \mathbf{x}} \left[\theta(\mathbf{x}) \rho^2(\mathbf{x}) \int_0^\infty (1 - e^{-\frac{\phi(r)}{\theta(\mathbf{x})}}) \frac{r^3}{3} \frac{\partial}{\partial r} Y(\theta(\mathbf{x}), r) dr \right]. \end{aligned} \quad (\text{B11})$$

The sum is, therefore,

$$\frac{2\pi}{3} \frac{\sigma^3}{m} \frac{1}{\rho(\mathbf{x})} \frac{\partial}{\partial \mathbf{x}} \left[\theta(\mathbf{x}) \rho^2(\mathbf{x}) \int_0^\infty (1 - e^{-\frac{\phi(r)}{\theta(\mathbf{x})}}) \frac{\partial}{\partial r} (r^3 Y(\theta(\mathbf{x}), r)) dr \right], \quad (\text{B12})$$

which is what appears in (38a).

2. Collision integral

Changing the dummy variable of integration $\mathbf{x}_2 = \mathbf{x} - \sigma \mathbf{r}$ in the collision integral of (35), we arrive at

$$\begin{aligned} & \frac{1}{m} \int e^{-\frac{\phi(\|\mathbf{x}-\mathbf{x}_2\|)}{\theta(\|\mathbf{x}+\mathbf{x}_2\|/2)}} Y_K(\theta(\|\mathbf{x}+\mathbf{x}_2\|/2), \|\mathbf{x}-\mathbf{x}_2\|) \lambda(\mathbf{z}-\mathbf{z}_2) [f(\mathbf{z}') f(\mathbf{z}'_2) - f(\mathbf{z}) f(\mathbf{z}_2)] d\mathbf{z}_2 \\ & = \frac{\sigma^3}{m} \int \left[f(\mathbf{x}, \mathbf{y}, \mathbf{v}'', \mathbf{w}'') f\left(\mathbf{x} - \frac{\sigma \mathbf{r}}{2}, \mathbf{y}_2, \mathbf{v}'_2, \mathbf{w}'_2\right) - f(\mathbf{x}, \mathbf{y}, \mathbf{v}, \mathbf{w}) f\left(\mathbf{x} - \frac{\sigma \mathbf{r}}{2}, \mathbf{y}_2, \mathbf{v}_2, \mathbf{w}_2\right) \right] \\ & \quad \times \lambda(\mathbf{r}, \mathbf{y} - \mathbf{y}_2, \mathbf{v} - \mathbf{v}_2, \mathbf{w} - \mathbf{w}_2) e^{-\frac{\phi(\|\mathbf{r}\|)}{\theta(\|\mathbf{x}-\sigma \mathbf{r}\|/2)}} Y_K(\theta(\|\mathbf{x}-\sigma \mathbf{r}\|/2), \|\mathbf{r}\|) dr dy_2 d\mathbf{v}_2 d\mathbf{w}_2, \end{aligned} \quad (\text{B13})$$

where the collision mappings are computed via (39). Taking the limit as $\sigma \rightarrow 0$, $K \rightarrow \infty$, and $\sigma^3/m \sim \text{constant}$, we further obtain

$$\begin{aligned} & \frac{\sigma^3}{m} \int \lambda(\mathbf{r}, \mathbf{y} - \mathbf{y}_2, \mathbf{v} - \mathbf{v}_2, \mathbf{w} - \mathbf{w}_2) e^{-\frac{\phi(\|\mathbf{r}\|)}{\theta(\mathbf{x})}} Y(\theta(\mathbf{x}), \|\mathbf{r}\|) \\ & \quad \times [f(\mathbf{x}, \mathbf{y}, \mathbf{v}'', \mathbf{w}'') f(\mathbf{x}, \mathbf{y}_2, \mathbf{v}'_2, \mathbf{w}'_2) - f(\mathbf{x}, \mathbf{y}, \mathbf{v}, \mathbf{w}) f(\mathbf{x}, \mathbf{y}_2, \mathbf{v}_2, \mathbf{w}_2)] dr dy_2 d\mathbf{v}_2 d\mathbf{w}_2 \\ & = \frac{\sigma^3}{m} \int \alpha(\mathbf{x}, \mathbf{r}, \mathbf{y} - \mathbf{y}_2, \mathbf{v} - \mathbf{v}_2, \mathbf{w} - \mathbf{w}_2) \\ & \quad \times [f(\mathbf{x}, \mathbf{y}, \mathbf{v}'', \mathbf{w}'') f(\mathbf{x}, \mathbf{y}_2, \mathbf{v}'_2, \mathbf{w}'_2) - f(\mathbf{x}, \mathbf{y}, \mathbf{v}, \mathbf{w}) f(\mathbf{x}, \mathbf{y}_2, \mathbf{v}_2, \mathbf{w}_2)] dr dy_2 d\mathbf{v}_2 d\mathbf{w}_2, \end{aligned} \quad (\text{B14})$$

which is what appears in (38b), with α given via (38c).

APPENDIX C: ENTROPY INEQUALITY FOR THE BOLTZMANN-VLASOV EQUATION

The computation of (47) proceeds as follows:

$$\begin{aligned} \langle \ln f \rangle_C(t, \mathbf{x}) & = \frac{1}{2} \int \alpha \ln \left(\frac{f(\mathbf{x}, \mathbf{y}, \mathbf{v}', \mathbf{w}') f(\mathbf{x}, \mathbf{y}_2, \mathbf{v}'_2, \mathbf{w}'_2)}{f(\mathbf{x}, \mathbf{y}, \mathbf{v}, \mathbf{w}) f(\mathbf{x}, \mathbf{y}_2, \mathbf{v}_2, \mathbf{w}_2)} \right) \\ & \quad \times f(\mathbf{x}, \mathbf{y}, \mathbf{v}, \mathbf{w}) f(\mathbf{x}, \mathbf{y}_2, \mathbf{v}_2, \mathbf{w}_2) dr dy_2 d\mathbf{v}_2 d\mathbf{w}_2 dy dv d\mathbf{w} \\ & = \frac{1}{2} \int \alpha \ln \left(\frac{f(\mathbf{x}, \mathbf{y}, \mathbf{v}', \mathbf{w}') f(\mathbf{x}, \mathbf{y}_2, \mathbf{v}'_2, \mathbf{w}'_2)}{f(\mathbf{x}, \mathbf{y}, \mathbf{v}, \mathbf{w}) f(\mathbf{x}, \mathbf{y}_2, \mathbf{v}_2, \mathbf{w}_2)} \right) \frac{f(\mathbf{x}, \mathbf{y}, \mathbf{v}, \mathbf{w}) f(\mathbf{x}, \mathbf{y}_2, \mathbf{v}_2, \mathbf{w}_2)}{f(\mathbf{x}, \mathbf{y}, \mathbf{v}', \mathbf{w}') f(\mathbf{x}, \mathbf{y}_2, \mathbf{v}'_2, \mathbf{w}'_2)} \\ & \quad \times f(\mathbf{x}, \mathbf{y}, \mathbf{v}', \mathbf{w}') f(\mathbf{x}, \mathbf{y}_2, \mathbf{v}'_2, \mathbf{w}'_2) dr dy_2 d\mathbf{v}_2 d\mathbf{w}_2 dy dv d\mathbf{w} \\ & \leq \frac{1}{2} \int \alpha \left(1 - \frac{f(\mathbf{x}, \mathbf{y}, \mathbf{v}, \mathbf{w}) f(\mathbf{x}, \mathbf{y}_2, \mathbf{v}_2, \mathbf{w}_2)}{f(\mathbf{x}, \mathbf{y}, \mathbf{v}', \mathbf{w}') f(\mathbf{x}, \mathbf{y}_2, \mathbf{v}'_2, \mathbf{w}'_2)} \right) \\ & \quad \times f(\mathbf{x}, \mathbf{y}, \mathbf{v}', \mathbf{w}') f(\mathbf{x}, \mathbf{y}_2, \mathbf{v}'_2, \mathbf{w}'_2) dr dy_2 d\mathbf{v}_2 d\mathbf{w}_2 dy dv d\mathbf{w} = 0. \end{aligned} \quad (\text{C1})$$

- [1] J. Boussinesq, *Essai sur la théorie des eaux courantes, Mémoires présentés par divers savants à l'Académie des Sciences* (Imprimerie Nationale, Paris, 1877).
- [2] O. Reynolds, An experimental investigation of the circumstances which determine whether the motion of water shall be direct or sinuous, and of the law of resistance in parallel channels, *Proc. R. Soc. London* **35**, 84 (1883).
- [3] A. N. Kolmogorov, Local structure of turbulence in an incompressible fluid at very high Reynolds numbers, *Dokl. Akad. Nauk SSSR* **30**, 299 (1941) [*Proc. R. Soc. Lond. A* **434**, 9 (1991)].
- [4] A. N. Kolmogorov, On degeneration of isotropic turbulence in an incompressible viscous liquid, *Dokl. Akad. Nauk SSSR* **31**, 538 (1941).
- [5] A. N. Kolmogorov, Energy dissipation in locally isotropic turbulence, *Dokl. Akad. Nauk SSSR* **32**, 19 (1941) [*Proc. R. Soc. Lond. A* **434**, 15 (1991)].
- [6] A. M. Obukhov, On the distribution of energy in the spectrum of a turbulent flow, *Bull. Acad. Sci. USSR, Geog. Geophys* **5**, 453 (1941).
- [7] L. F. Richardson, Atmospheric diffusion shown on a distance-neighbour graph, *Proc. R. Soc. London A* **110**, 709 (1926).
- [8] G. I. Taylor, Statistical theory of turbulence, *Proc. R. Soc. London A* **151**, 421 (1935).
- [9] G. I. Taylor, The spectrum of turbulence, *Proc. R. Soc. London A* **164**, 476 (1938).
- [10] T. de Karman and L. Howarth, On the statistical theory of isotropic turbulence, *Proc. R. Soc. London A* **164**, 192 (1938).
- [11] L. Prandtl, Beitrag zum Turbulenzsymposium, in *Proceedings of the Fifth International Congress on Applied Mechanics*, edited by J.P. Den Hartog and H. Peters (Wiley, New York, 1938), pp. 340–346.
- [12] A. M. Obukhov, Structure of the temperature field in turbulent flow, *Izv. Akad. Nauk SSSR Ser. Geogr. Geofiz.* **13**, 58 (1949).
- [13] S. Chandrasekhar, On Heisenberg's elementary theory of turbulence, *Proc. R. Soc.* **200**, 20 (1949).
- [14] S. Corrsin, On the spectrum of isotropic temperature fluctuations in an isotropic turbulence, *J. Appl. Phys.* **22**, 469 (1951).
- [15] A. N. Kolmogorov, A refinement of previous hypotheses concerning the local structure of turbulence in a viscous incompressible fluid at high Reynolds number, *J. Fluid Mech.* **13**, 82 (1962).
- [16] A. M. Obukhov, Some specific features of atmospheric turbulence, *J. Geophys. Res.* **67**, 3011 (1962).
- [17] R. H. Kraichnan, Isotropic turbulence and inertial range structure, *Phys. Fluids* **9**, 1728 (1966).
- [18] R. H. Kraichnan, Dispersion of particle pairs in homogeneous turbulence, *Phys. Fluids* **9**, 1937 (1966).
- [19] P. G. Saffman, The large-scale structure of homogeneous turbulence, *J. Fluid Mech.* **27**, 581 (1967).
- [20] P. G. Saffman, A model for inhomogeneous turbulent flow, *Proc. R. Soc. London A* **317**, 417 (1970).
- [21] B. B. Mandelbrot, Intermittent turbulence in self-similar cascades; divergence of high moments and dimension of the carrier, *J. Fluid Mech.* **62**, 331 (1974).
- [22] K. Avila, D. Moxey, A. de Lozar, M. Avila, D. Barkley, and B. Hof, The onset of turbulence in pipe flow, *Science* **333**, 192 (2011).
- [23] H. H. Khan, S. F. Anwer, N. Hasan, and S. Sanghi, Laminar to turbulent transition in a finite length square duct subjected to inlet disturbance, *Phys. Fluids* **33**, 065128 (2021).
- [24] R. V. Abramov, Macroscopic turbulent flow via hard sphere potential, *AIP Adv.* **11**, 085210 (2021).
- [25] R. V. Abramov, Turbulence in large-scale two-dimensional balanced hard sphere gas flow, *Atmosphere* **12**, 1520 (2021).
- [26] N. N. Bogoliubov, Kinetic equations, *J. Exp. Theor. Phys.* **16**, 691 (1946).
- [27] M. Born and H. S. Green, A general kinetic theory of liquids I: The molecular distribution functions, *Proc. R. Soc. A* **188**, 10 (1946).
- [28] J. G. Kirkwood, The statistical mechanical theory of transport processes I: General theory, *J. Chem. Phys.* **14**, 180 (1946).
- [29] A. A. Vlasov, On vibration properties of electron gas, *Zh. Eksp. Teor. Fiz.* **8**, 291 (1938) [*Sov. Phys. Usp.* **10**, 721 (1968)].
- [30] S. Tsugé, Approach to the origin of turbulence on the basis of two-point kinetic theory, *Phys. Fluids* **17**, 22 (1974).
- [31] R. V. Abramov, Turbulent energy spectrum via an interaction potential, *J. Nonlinear Sci.* **30**, 3057 (2020).

- [32] X. Jia, Y.-K. Choi, B. Mourrain, and W. Wang, An algebraic approach to continuous collision detection for ellipsoids, *Computer Aided Geom. Design* **28**, 164 (2011).
- [33] R. V. Abramov, The random gas of hard spheres, *J* **2**, 162 (2019).
- [34] H. Grad, On the kinetic theory of rarefied gases, *Commun. Pure Appl. Math.* **2**, 331 (1949).
- [35] F. Papangelou, Integrability of expected increments of point processes and a related random change of scale, *Trans. Amer. Math. Soc.* **165**, 483 (1972).
- [36] D. J. Daley and D. Vere-Jones, *An Introduction to the Theory of Point Processes. Volume I: Elementary Theory and Methods*, 2nd ed. (Springer, Berlin, 2003).
- [37] P. Courrège, Sur la forme intégréo-différentielle des opérateurs de C_k^∞ dans C satisfaisant au principe du maximum, *Séminaire Brelot-Choquet-Deny. Théorie du potentiel* **10**, 1 (1965-1966).
- [38] I. I. Gikhman and A. V. Skorokhod, *Introduction to the Theory of Random Processes* (Dover, New York, 1969).
- [39] W. Feller, *An Introduction to Probability Theory and its Applications, Volume 2*, 2nd ed. (Wiley, New York, 1971).
- [40] D. Applebaum, *Lévy Processes and Stochastic Calculus*, 2nd ed., Cambridge Studies in Advanced Mathematics No. 116 (Cambridge University Press, Cambridge, 2009).
- [41] C. E. Shannon, A mathematical theory of communication, *Bell System Tech. J.* **27**, 379 (1948).
- [42] S. Kullback and R. Leibler, On information and sufficiency, *Ann. Math. Statist.* **22**, 79 (1951).
- [43] T. Boublík, Background correlation functions in the hard sphere systems, *Mol. Phys.* **59**, 775 (1986).
- [44] T. Boublík, Hard-sphere radial distribution function from the residual chemical potential, *Mol. Phys.* **104**, 3425 (2006).
- [45] C. Cercignani, R. Illner, and M. Pulvirenti, The mathematical theory of dilute gases, *Applied Mathematical Sciences*, Vol. 106 (Springer, Berlin, 1994).
- [46] L. Boltzmann, Weitere Studien über das Wärmegleichgewicht unter Gasmolekülen, *Sitz.-Ber. Kais. Akad. Wiss. (II)* **66**, 275 (1872).
- [47] S. Chapman and T. G. Cowling, *The Mathematical Theory of Non-Uniform Gases*, 3rd ed., Cambridge Mathematical Library (Cambridge University Press, Cambridge, 1991).
- [48] J. O. Hirschfelder, C. F. Curtiss, and R. B. Bird, *The Molecular Theory of Gases and Liquids* (Wiley, New York, 1964).
- [49] M. Lachowicz, On the hydrodynamic limit of the Enskog equation, *Publ. Res. Inst. Math. Sci.* **34**, 191 (1998).
- [50] G. K. Batchelor, *An Introduction to Fluid Dynamics* (Cambridge University Press, New York, 2000).
- [51] F. Golse, *The Boltzmann Equation and its Hydrodynamic Limits* (Elsevier, Amsterdam, 2005), Chap. 3, pp. 159–301.
- [52] H. Yamaguchi, P. Perrier, M. T. Ho, J. G. Méolans, T. Niimi, and I. Graur, Mass flow rate measurement of thermal creep flow from transitional to slip flow regime, *J. Fluid Mech.* **795**, 690 (2016).
- [53] S. Duhr and D. Braun, Why molecules move along a temperature gradient, *Proc. Natl. Acad. Sci. USA* **103**, 19678 (2006).
- [54] P. Buchhave and C. M. Velte, Measurement of turbulent spatial structure and kinetic energy spectrum by exact temporal-to-spatial mapping, *Phys. Fluids* **29**, 085109 (2017).
- [55] H. G. Weller, G. Tabor, H. Jasak, and C. Fureby, A tensorial approach to computational continuum mechanics using object-oriented techniques, *Comput. Phys.* **12**, 620 (1998).
- [56] C. J. Greenshields, H. G. Weller, L. Gasparini, and J. M. Reese, Implementation of semi-discrete, non-staggered central schemes in a colocated, polyhedral, finite volume framework, for high-speed viscous flows, *Int. J. Numer. Methods Fluids* **63**, 1 (2010).
- [57] A. Kurganov and E. Tadmor, New high-resolution central schemes for nonlinear conservation laws and convection–diffusion equations, *J. Comput. Phys.* **160**, 241 (2000).
- [58] B. van Leer, Towards the ultimate conservative difference scheme, II: Monotonicity and conservation combined in a second order scheme, *J. Comput. Phys.* **14**, 361 (1974).
- [59] A. J. Majda and I. Timofeyev, Remarkable statistical behavior for truncated Burgers–Hopf dynamics, *Proc. Natl. Acad. Sci. USA* **97**, 12413 (2000).

- [60] R. V. Abramov, Statistically relevant and irrelevant conserved quantities for the equilibrium statistical description of the truncated Burgers–Hopf equation and the equations for barotropic flow, Ph.D. thesis, Rensselaer Polytechnic Institute, 2002.
- [61] G. D. Nastrom and K. S. Gage, A climatology of atmospheric wavenumber spectra of wind and temperature observed by commercial aircraft, *J. Atmos. Sci.* **42**, 950 (1985).
- [62] D. S. Choi and A. P. Showman, Power spectral analysis of Jupiter’s clouds and kinetic energy from *Cassini*, *Icarus* **216**, 597 (2011).
- [63] M. L. Moriconi, A. Migliorini, F. Altieri, A. Adriani, A. Mura, G. Orton, J. I. Lunine, D. Grassi, S. K. Atreya, A. P. Ingersoll, B. M. Dinelli, S. J. Bolton, S. Levin, F. Tosi, R. Noschese, C. Plainaki, A. Cicchetti, G. Sindoni, and A. Olivieri, Turbulence power spectra in regions surrounding Jupiter’s south polar cyclones from *Juno/JIRAM*, *J. Geophys. Res. Planets* **125**, e2019JE006096 (2020).